JOURNAL OF GEOPHYSICAL RESEARCH, VOL. 105, NO. D2, PAGES 1889–1908, JANUARY 27, 2000

A nonurban ozone air pollution episode over eastern China: Observations and model simulations

C. Luo,[1] J. C. St. John,[1] Zhou Xiuji,[2] K. S. Lam,[3]
T. Wang,[3] and W. L. Chameides[1]

Abstract. Air quality data gathered from five nonurban sites in China over a 12-month period from August 1994 to August 1995, along with meteorological observations from the same region and period, are used to identify and characterize a nonurban ozone (O_3) pollution episode in China. Because of the influence of the Asian Monsoonal Circulation, high O_3 concentrations were not observed at the nonurban sites during the summer months. However, enhanced O_3 concentrations were observed during the other seasons, especially the fall and early winter. A more detailed inspection of the O_3 data during the period from October 15, 1994, to January 15, 1995, indicated the occurrence of a multiple-day episode in late October/early November when high O_3 concentrations were observed at all four monitoring sites located in eastern China. Meteorological conditions during the episode were characterized by the presence of a strong and stationary high-pressure ridge over eastern China; synoptic conditions quite similar to those observed during regional O_3 pollution episodes over the United States, Canada, and Europe. An updated version of the Regional Acid Deposition Model (RADM) driven by meteorological fields derived from the Regional Climate Model (RegCM) and spatially disaggregated anthropogenic emissions prepared by the Chinese Academy of Meteorological Sciences is used to simulate 3 months of the observed O_3 data from China. Comparisons between observations and model calculations indicate that the model is able to reproduce some of the key features of the O_3 distribution and its relationship to the concentration of one primary pollutant (i.e., sulfur dioxide) provided the comparison is made using averaging times of several days or more. However, simulation of day-to-day variations in O_3 at a given site was poorly correlated with observations. Model simulations suggest that peak O_3 concentrations during this episode would respond to changes in NO_x and VOC emissions in a spatially inhomogeneous manner. In general, rural areas in southern China tend to be NO_x-limited, but rural areas in northern China tend to be VOC-limited. The Yangtze Delta region, where the highest O_3 concentrations were observed and predicted to occur, was found to be transitional between VOC and NO_x limitation.

1. Introduction

Tropospheric ozone (O_3) is produced in the atmosphere by a complex set of chemical reactions known as the photochemical smog mechanism. This mechanism involves the oxidation of volatile organic compounds (VOC) and carbon monoxide in the presence of nitrogen oxides (NO_x) and sunlight [*Haagen-Smit and Fox*, 1956; *National Research Council* (*NRC*), 1991]. In industrialized regions of the world, anthropogenic emissions of VOC and NO_x can amplify the photochemical smog process, thereby leading to air pollution episodes with enhanced concentrations of O_3 at the ground [e.g., *Korth*, 1963; *Altschuller et al.*, 1967; *NRC*, 1991]. While such air pollution episodes are usually most intense within high population/industrialized centers, the full spatial extent of enhanced O_3 concentrations during these episodes can be thousands of kilometers, encompassing rural and agricultural areas as well as urban centers [*NRC*, 1991]. In addition to causing damage to forests and crops [*Lefohn*, 1992; *Chameides et al.*, 1994], these "nonurban O_3 pollution episodes" can facilitate the long-range transport of pollutants between urban source areas [*Wolff and Lioy*, 1980] and between urban source areas and the remote troposphere [*Jacob et al.*, 1996].

While the frequency and characteristics of nonurban O_3 pollution have been studied extensively in many industrially developed regions (e.g., the Canadian/United States subcontinent and Europe) [*Vukovich et al.*, 1977; *Vukovich*, 1979; *King and Vukovich*, 1982; *Fishman et al.*, 1987; *Samson and Shi*, 1989; *Davies et al.*, 1992; *Vukovich*, 1995; *Millán et al.*, 1996], little is known of these episodes over the Chinese subcontinent. Recently, *Chameides et al.* [1999] analyzed O_3 data gathered at four nonurban sites in China during 1994 and 1995. These authors found episodes with enhanced O_3 concentrations at these sites to be most frequent in the fall and early winter and conjectured, on the basis of these data, that regional O_3 pollution may be affecting the yields of winter wheat grown in China.

In this work, we present a more detailed examination of the nonurban O_3 data from China discussed by *Chameides et al.*

[1]School of Earth and Atmospheric Sciences, Georgia Institute of Technology, Atlanta.
[2]Chinese Academy of Meteorological Sciences, Beijing, China.
[3]Department of Civil and Structural Engineering, Hong Kong Polytechnic University, Hong Kong, China.

Paper number 1999JD900970.
0148-0227/00/1999JD900970$09.00

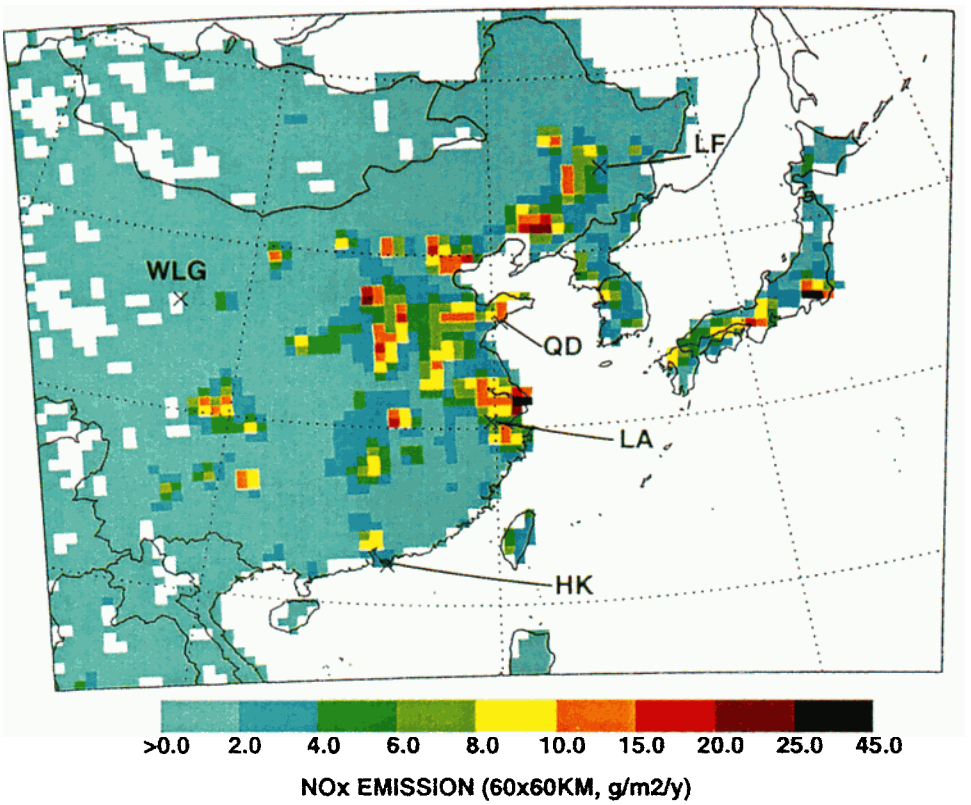

Plate 1. Spatial distribution of anthropogenic NO_x emissions over the East Asian domain used in our regional model simulations. The emissions are from the inventories of *Bai* [1996] for China and *Kato and Akimoto* [1992] for Japan and North and South Korea and have been aggregated into the 60 × 60 km grid of our regional model. Also shown on the plate are the locations of the five monitoring sites where nonurban air quality data used in our analysis were collected.

[1999]. Using the air quality data from these same nonurban monitoring sites, standard meteorological data from China, and an updated version of the Regional Acid Deposition Model (RADM) [*Chang et al.*, 1987], we identify and characterize the meteorological and chemical properties of a multiple-day, apparently region-wide, nonurban O_3 pollution episode that occurred in eastern China in the fall of 1994.

In the discussion below, we begin with a brief summary of our current understanding of O_3 pollution in China and the possible regional extent of this pollution. This is followed by an examination of nonurban air quality and meteorological data observed over China during a 12-month period from August 1994 to August 1995. We then conclude with a presentation of RADM simulations of nonurban air quality in eastern China during a 3-month segment of the 12-month period when nonurban O_3 concentrations tended to be at their peak. Distinctive aspects of the model calculations are (1) the relatively long 3-month simulation period, which affords an evaluation of model performance over timescales ranging from daily to seasonal, and (2) the simulation of an O_3 episode during the late fall, which allows us to assess O_3 precursor relationships under relatively low actinic flux conditions.

2. Evidence of O_3 Pollution in China

China, the most populous nation in the world, has experienced a decade of rapid economic expansion and industrial development [*United Nations* (*U. N.*), 1991; *Elliott et al.*, 1997; *Chameides et al.*, 1999]. As a result of this development, anthropogenic emissions associated with the burning of fossil fuels from China have grown significantly in recent years [*Smil*, 1993] and in many cases are now believed to be comparable in magnitude to those from the United States and Europe. For example, estimates of anthropogenic NO_x emissions in China range from 0.3 to 1.1 kg N km^{-2} d^{-1} [*Galloway et al.*, 1994; *Bai*, 1996], while in the United States estimates are about 1.7 kg N km^{-2} d^{-1} and in Europe are about 1.5 to 3.5 kg N km^{-2} d^{-1} [*U.S. Environmental Protection Agency* (*EPA*), 1998; *Chameides et al.*, 1994]. Moreover, the emissions in China are dispersed along the eastern coast, as well as along the Yangtze and Yellow Rivers and in the Sichuan valley (see Plate 1). Given this situation, it is not surprising that high O_3 concentrations (e.g., in excess of 120 ppbv) have been observed in China's urban centers [e.g., *Tang et al.*, 1986; Z. X. Shan, private communication, 1998], and, by extension, one would expect to find the occurrence of nonurban O_3 pollution episodes as well.

However, while the magnitude of anthropogenic NO_x emissions in China suggests that nonurban O_3 pollution episodes like those observed in more developed western nations occur in China, other aspects of the Chinese situation are quite different from those found in these other areas of the globe. One of these differences relates to meteorology. Along with sufficient precursor emissions the existence of meteorological conditions that promote the formation and accumulation of air pollutants is a necessary condition for the occurrence of an O_3 pollution episode. In areas such as the United States, Canada, and Europe this meteorology often includes the presence of

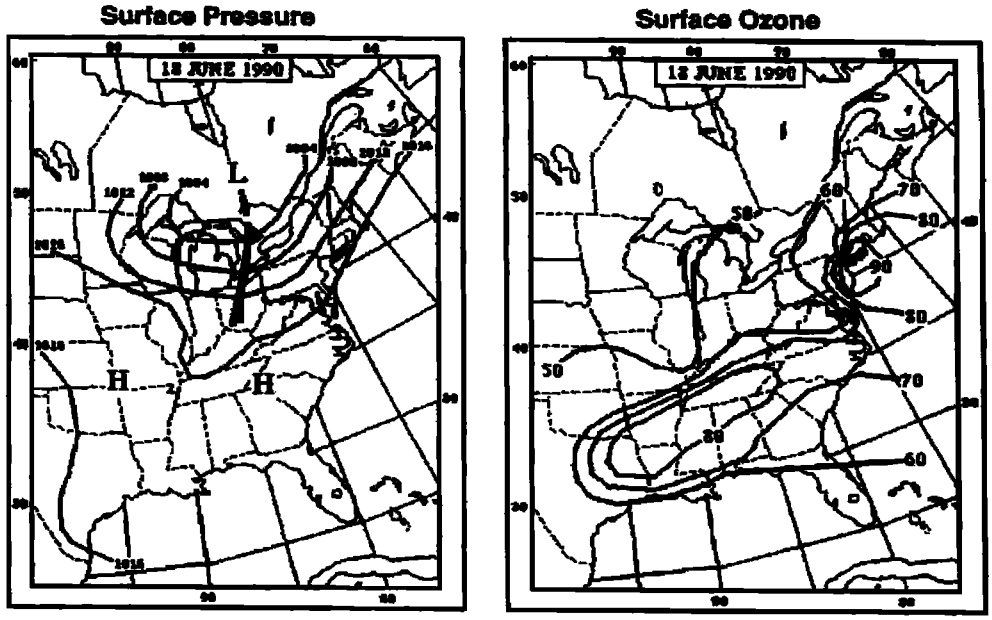

Figure 1. Meteorological conditions and O_3 concentrations during a regional air pollution episode over the eastern United States in August 1995 [from *Vukovich*, 1995].

slow moving high-pressure systems [*Vukovich et al.*, 1977; *Vukovich*, 1979, 1994, 1995; *King and Vukovich*, 1982; *Fishman et al.*, 1987; *Samson and Shi*, 1989; *Davies et al.*, 1992; *Millán et al.*, 1996; *Davis et al.*, 1998]. The clear skies typical of these systems favor high boundary layer temperatures and actinic fluxes and thus an acceleration of the photochemical smog mechanism [*Dodge*, 1989; *Cardelino and Chameides*, 1990]. The vertical stability of these systems tends to depress vertical mixing and boundary layer venting, thereby allowing O_3 and its precursor compounds to accumulate near the surface. Because these systems are often slow moving, photochemically produced O_3 can build up over a series of days, thereby producing a multiday, air pollution episode. Moreover, the synoptic nature of these systems affords conditions favorable for the production and buildup of O_3 and related pollutants over large spatial scales, giving rise to region-wide or regional air pollution episodes.

Of the various types of high-pressure configurations that might foster a multiple-day, regional O_3 pollution episode, one commonly encountered is illustrated in Figure 1, a depiction of the weather patterns and corresponding peak surface O_3 concentrations encountered during a typical episode over the eastern United States [*Vukovich*, 1995]. Of particular relevance to our later discussions is the fact that in this type of episode the region is dominated by two high-pressure centers. Moreover, the area of enhanced O_3 concentrations over the southeastern United States does not overlay the two high-pressure centers but rather the ridge of high pressure connecting these two centers. It is also relevant to note that the horizontal pressure gradients, and thus the synoptic forcing along this ridge, are extremely weak.

Because high-pressure systems with hot, stagnant conditions tend to be most frequent over much of the industrially developed areas of the West during the late spring and summer, the most severe and widespread O_3 pollution episodes over these areas generally occur during these months [e.g., *NRC*, 1991; *United Kingdom (U.K.) Report*, 1997; *Scheel et al.*, 1997]. (Exceptions to this trend appear to become more frequent as one moves to more southern latitudes, where wintertime temperatures and actinic fluxes can be substantial. Thus fall and even wintertime O_3 pollution episodes are not uncommon in Houston and Los Angeles [*Davis et al.*, 1998; South Coast Air Quality Management District (SCAQMD) Web site, http://www.aqmd.gov/smog/, 1998], and O_3 pollution episodes in Mexico City are most frequent during the winter [*Secretaria de Medio Ambiente, Recursos Naturales y Pesca (SEMARNAP)*, 1997].)

In China, however, a very different situation applies. Meteorological conditions during the late spring and summer are dominated by the Asian Monsoonal Circulation. This circulation subjects the subcontinent to unstable conditions, with clouds, boundary layer venting, and copious rainfall [*Ding*, 1992; *Grotjahn*, 1993]; conditions that are not favorable to the formation and accumulation of air pollutants. This suggests that nonurban O_3 pollution episodes may not be common over China during the late spring and summer. Indeed, *Wang et al.* [1997] found O_3 concentrations at their Hong Kong station to be at their lowest during the summer. A major focus of this work will be to determine whether meteorological conditions ever exist in China that favor the occurrence of nonurban O_3 pollution episodes, and if so, the timing and characteristics of the resulting episodes.

3. Observational Data

Our analysis combines meteorological data with surface atmospheric chemical measurements made at nonurban sites in China to, first, identify a specific nonurban O_3 pollution episode, and then infer its characteristics through diagnostic analysis and model simulations. In the discussion below, the salient aspects of these data are discussed.

3.1. Meteorological Data

Our inferences on the meteorological characteristics of nonurban air pollution episodes in China are based on measurements of surface pressure, temperature, precipitation, and wind direction at relevant meteorological stations, with data reported in accordance with the protocols of the World Me-

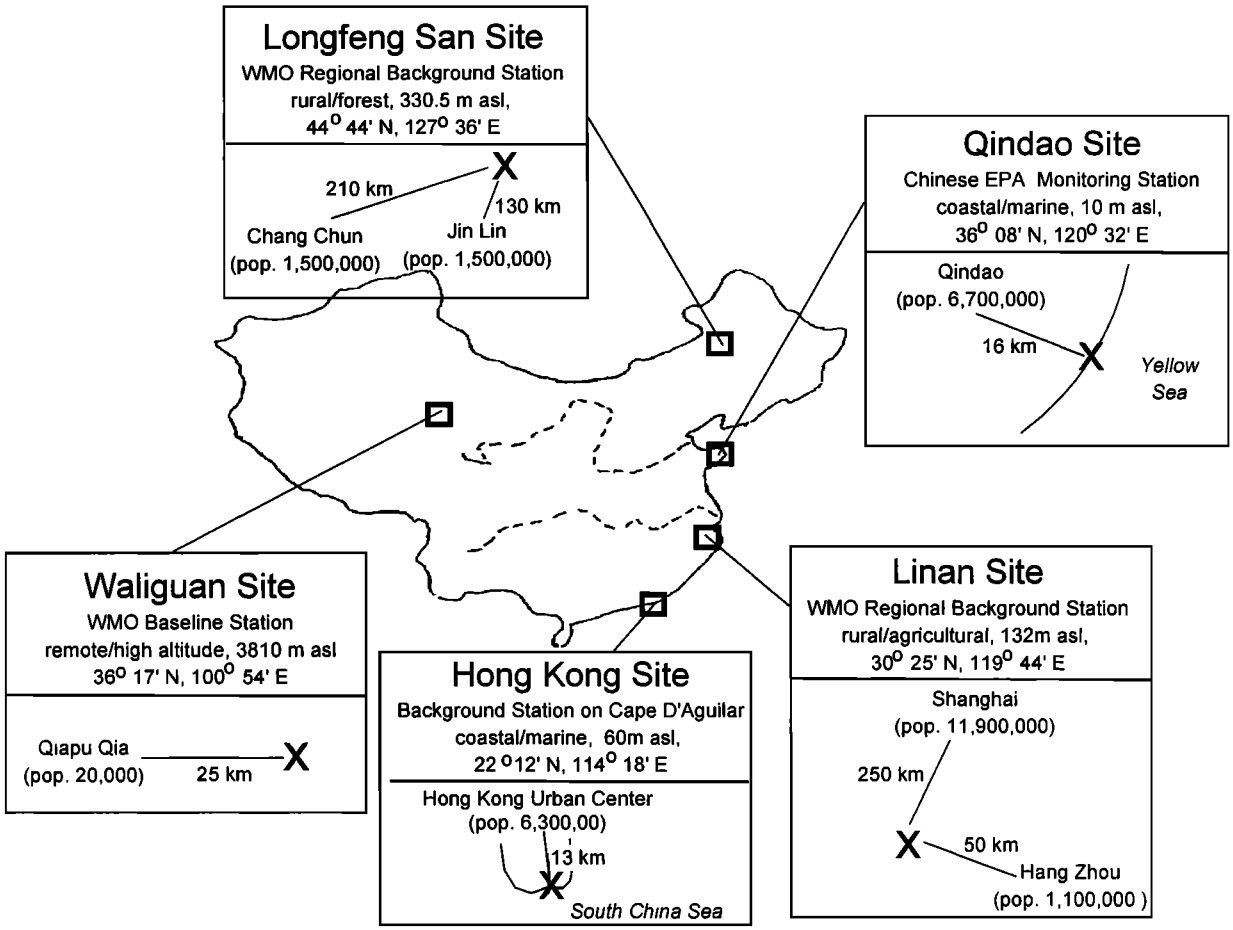

Figure 2. Locations of the five nonurban monitoring sites. Insets: characteristics of each site and the directions and distances to each site's most proximate and significant sources of pollutants, with crosses indicating the location of the site.

teorological Organization. Daily mean surface pressures (corrected to sea level), temperatures, and total daily precipitation measured at nearly 1000 East Asian, surface meteorological stations were acquired from the U.S. National Climatic Data Center's archive of "summary of the day" data sets.

3.2. Atmospheric Chemical Data

The atmospheric chemical data used in our study were collected at five nonurban sites in China (Figure 2). Four of these sites (Longfeng San, Qindao, Linan, and Waliguan) were operated over a 12-month period beginning in mid-August 1994 as part of the Chinese Ozone Research Program (CORP), a research project carried out by the Chinese Academy of Meteorological Sciences with support from the National Natural Research Foundation of China [*Peng et al.*, 1997]. The fifth site at Cape D'Aguilar, Hong Kong, has been operated since November 1993 by the Hong Kong Polytechnic University [*Wang et al.*, 1997]. Our analysis uses 1-hour averages of the measurements of O_3 and sulfur dioxide (SO_2) at the CORP sites over the 12-month period, as well as limited measurements of volatile organic carbon (VOC) at three of the CORP sites. Hourly averaged O_3 observations from the Hong Kong site over the same period were also included. Ground-level O_3 concentrations at each site were measured using a TECO-49 ultraviolet O_3 analyzer (at Linan, a Dasibi was used for a 2-month period). The SO_2 measurements were made using a TECO-42s or 43s SO_2 monitor. The VOC concentrations were determined by gas chromatographic/flame ionization detection of five whole-air grab samples collected on 5 separate days at each of the sites during the fall of 1994.

3.3. Site Characteristics

The five sites, illustrated in Figure 2, encompass a variety of land uses, with one in a remote, high-altitude region of west central China (i.e., Waliguan) and the other four along an approximate north-south meridian in eastern China, where most of the anthropogenic emissions of O_3 precursors occur (see Plate 1). Of the four eastern sites, the northernmost, Longfeng San, was the most remote, situated in a forest within Heilongjiang Province and distant from major population and industrial centers. The most proximate sources of anthropogenic emissions to the Longfeng San site are Jinlin about 130 km to the south-southwest and Changchun about 210 km to the southwest. The populations of these cities are both of the order of 1.5 million. The Qindao site was situated on the coast of the Yellow Sea, just 16 km southeast of city of Qindao (population of ~6.7 million) and its associated pollutant emissions. The Linan site was situated about 10 km north of the Linan county township (population of 50,000), and 50 and 250 km northwest and southwest of the major population centers of Hangzhou

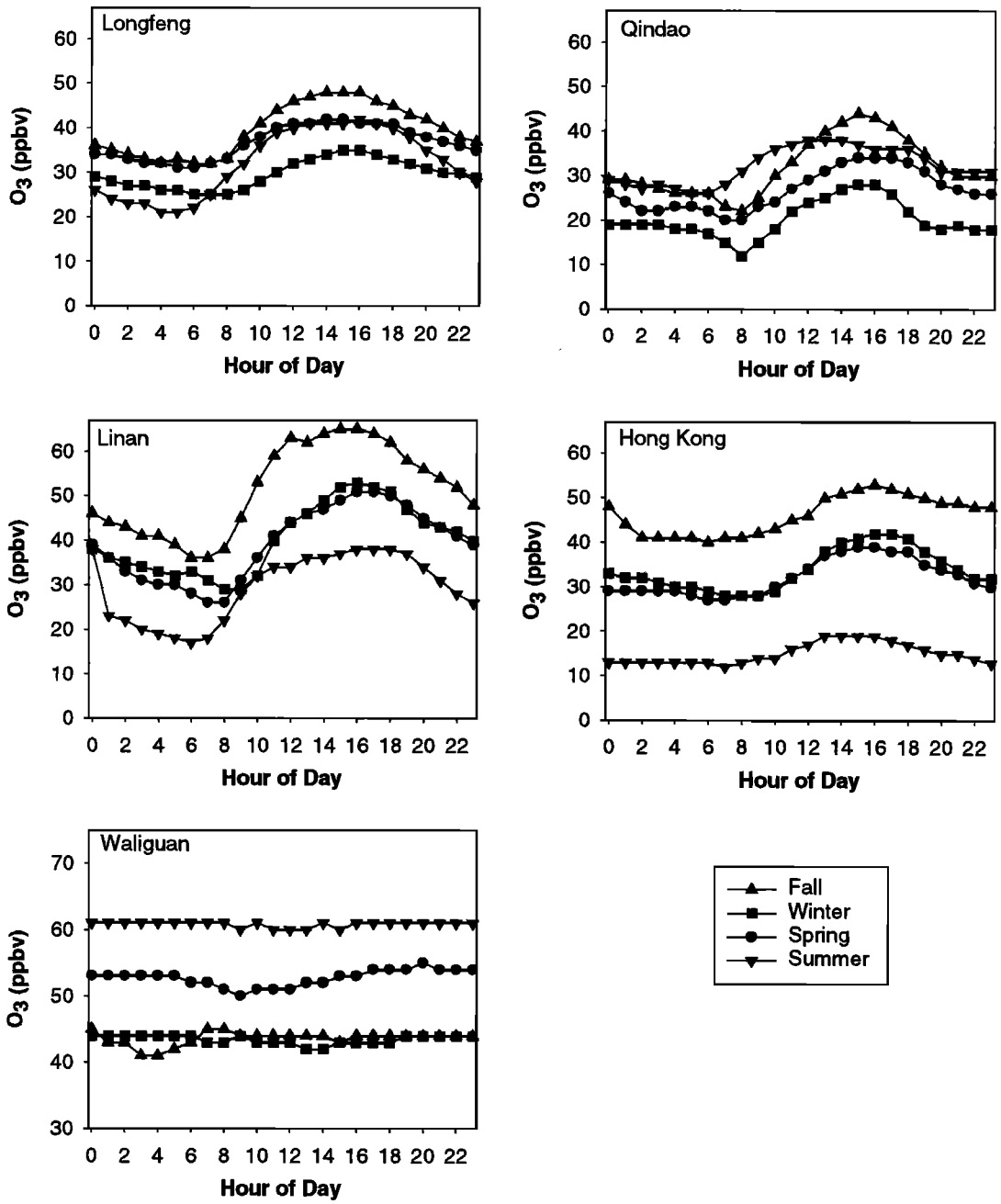

Figure 3. Seasonally averaged O_3 as a function of time of day observed at Langfeng San, Qindao, Linan, Hong Kong, and Waliguan.

and Shanghai, respectively. Nevertheless, the immediate area around the site is quite rural and the home of significant agricultural activity. The Hong Kong site is located on the southeastern tip of Hong Kong Island. While the urban center of Hong Kong, on Kowloon, is only about 13 km to the north, the prevailing winds at the site are out of the east and thus coming from the sea. For this reason, the data from the Hong Kong site reflect relatively remote, marine conditions, with intermittent urban-like air pollution episodes [*Wang et al.*, 1997, 1998].

4. Ozone Data From the Five Nonurban Sites

Further insight into the chemical characteristics of the sites can be obtained from the average diurnal variation in O_3 observed at each of the sites (Figure 3). The four eastern sites show qualitatively similar diurnal patterns, with maxima in the late afternoon and minima in the early morning hours preceding dawn. This pattern is, in fact, typical of rural sites in other regions of the globe and reflects a combination of photochemical production and downward transport of O_3-rich air from above during the daylight hours causing the O_3 peak, and dry deposition and chemical loss causing the minimum at night [*Logan*, 1989].

In contrast to that of the four eastern sites, O_3 from the Waliguan site exhibits almost no diurnal variation, with slightly higher concentrations at night than during the day. This type of pattern is typical of high-altitude sites [*Logan*, 1989]. The nocturnal maximum in O_3 at high altitude sites such as Waliguan

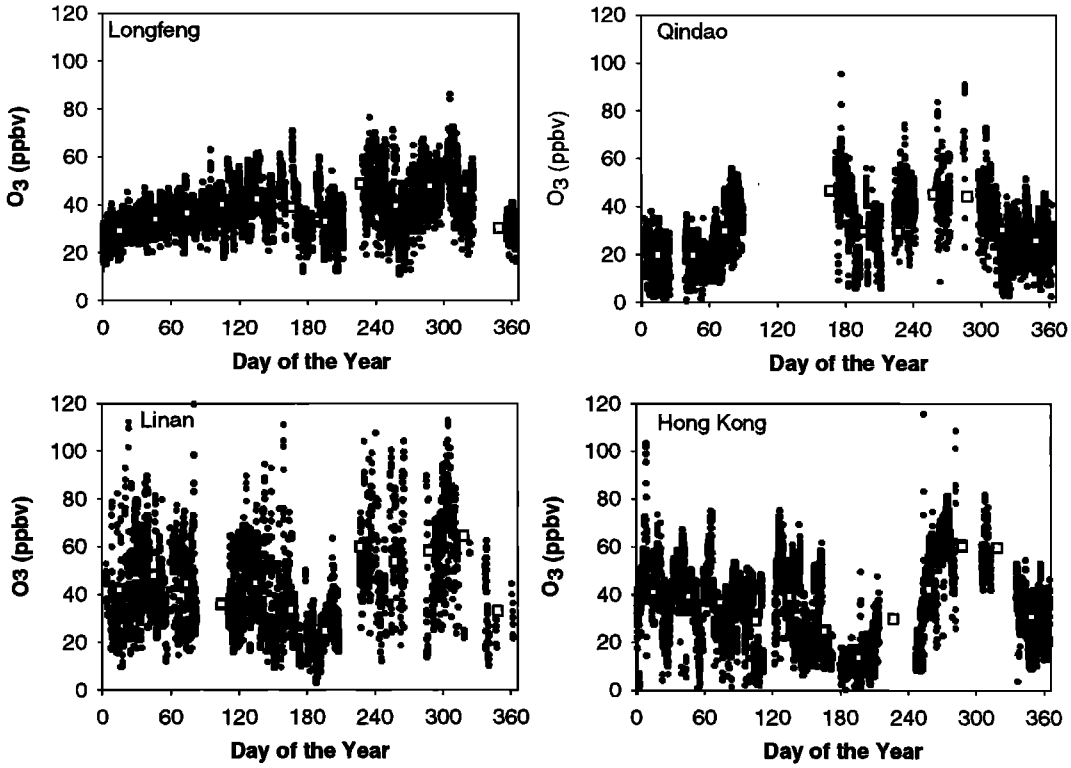

Figure 4. Hourly averaged O_3 observed between 0800 and 2000 hours (plusses) and monthly averaged O_3 (squares) as a function of Julian Date at the four sites in eastern China [after *Chameides et al.*, 1999].

reflects the fact that these sites generally lie above the boundary layer at night. Under these conditions the site is directly exposed to free tropospheric air and is insulated from loss via dry deposition to the surface. As a result, O_3 concentrations tend to peak during the nighttime hours. Because of the altitude of the Waliguan site as well as its remote, western location, the data from this site cannot be used to document the occurrence of nonurban O_3 pollution episodes in China. On the other hand, because, on average, the nighttime data from the Waliguan site reflect free tropospheric O_3 concentrations over that part of the globe, these data can be used to help substantiate that high ground-level O_3 concentrations observed at the other sites were indicative of a boundary layer source as opposed to downward transport from above.

The data illustrated in Figure 3 also illustrate the seasonal variation of O_3 in rural China during the 1994/1995 monitoring period considered here. Inspection of the figure reveals that on a seasonally averaged basis the highest O_3 concentrations at the four eastern sites occurred during the fall. (As discussed in the previous section, this trend contrasts to that typically found in most locales in the United States, Canada, and Europe, where peak surface O_3 usually occurs during the late spring and summer, and is most likely due to the influence of the Asian Monsoonal Circulation.) A more detailed depiction of the observed variability in O_3 is provided in Figure 4 where hourly and monthly averaged O_3 concentrations measured between 0800 and 2000 hours are plotted as a function of Julian Date. Similar to Figure 3, the data illustrated in Figure 4 indicate that peak monthly averaged daytime O_3 concentrations at the four eastern sites during the sampling period tended to occur during the fall months. It is also apparent that episodes with enhanced O_3 concentrations at one or more of the four eastern sites were most frequent during the fall and early wintertime. In the next section we focus in more detail on this fall/early winter period.

5. Identification of a Regional-Scale, Nonurban O_3 Pollution Episode

In Figure 5 the daily peak O_3 concentrations observed at each of the monitoring sites, as well as seasonal trend lines obtained from a polynomial regression, are plotted as a function of day from October 15, 1994, to January 15, 1995. (Figure 5 also depicts model-calculated peak O_3 concentrations; these will be discussed in a subsequent section.) Inspection of the figure reveals a number of episodes when peak O_3 concentrations at one or more of the sites spiked upward for a day or more. There is one period, however, of particular interest: a 13-day interval from October 26 to November 7 when all four eastern sites experienced enhanced O_3 at more or less the same time. In fact, there may have been additional episodes with simultaneous enhancements of O_3 at the eastern sites, but large gaps in the data from Longfeng San and Linan make identification of them problematic.

The late October/early November episode appears to have reached its maximum intensity during the first 2 days of November when Linan, Qindao, and Longfeng San all experienced their highest daily peak O_3 concentrations of the 13-day period; that is, 112 ppbv at Linan on November 1, 67 ppbv at Qindao on November 1, and 86 ppbv at Longfeng San on November 2. Perhaps because of its more southerly location, the day-to-day variation in O_3 at Hong Kong appears to have been somewhat decoupled from that of the other sites. Thus, while O_3 concentrations were reaching their apex at Linan,

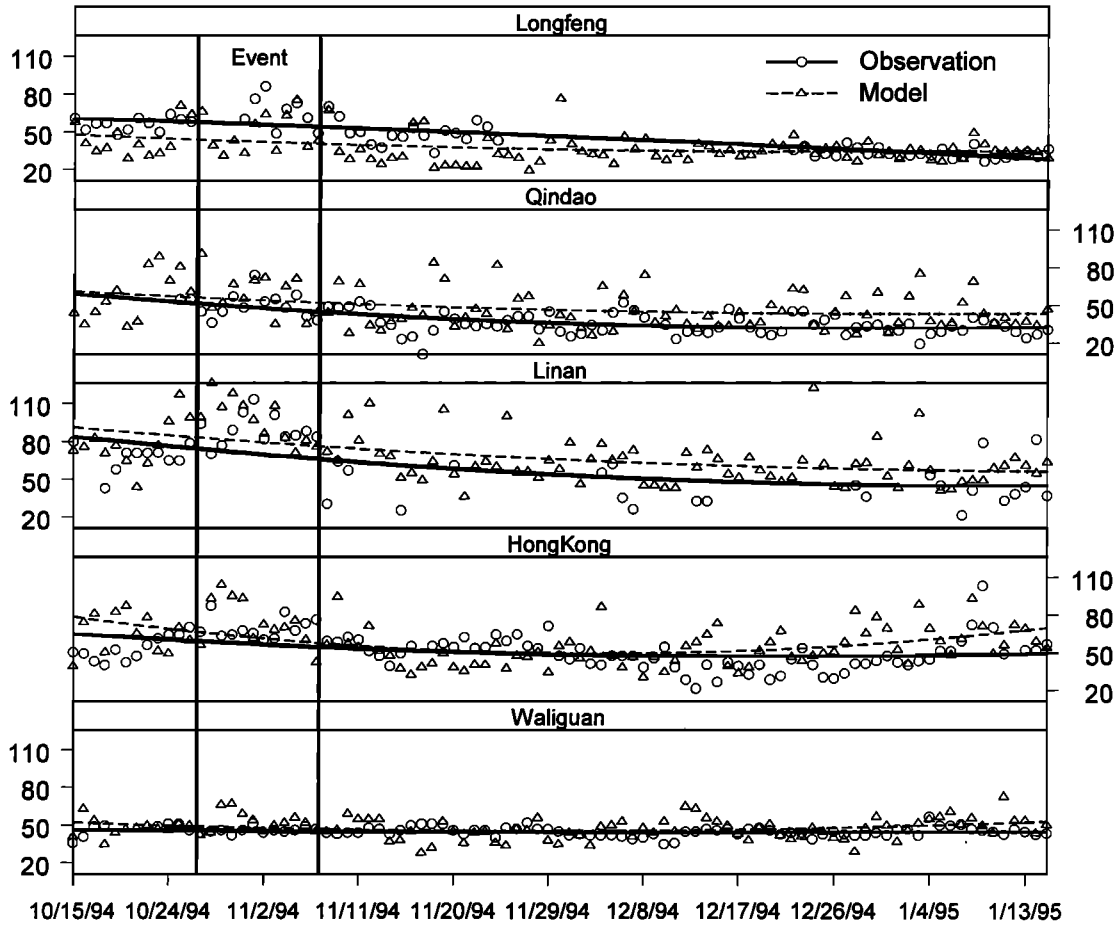

Figure 5. Observed and model-calculated daily maximum O_3 concentrations at the five monitoring sites over the 3-month period from October 15, 1994, to January 15, 1995. The circles and triangles represent the daily observations, and the lines represent polynomial regressions of the observed and modeled maxima to provide an estimate of the seasonally dependent average concentration at each site. The vertical lines delineate a 13-day episode with enhanced O_3 concentrations that is the focus of more detailed analysis.

Qindao, and Longfeng San on November 1 and 2, O_3 at Hong Kong was fairly close to its seasonal average. Hong Kong's highest daily peak O_3 concentration of 87 ppbv was observed on October 28, when O_3 concentrations at the other sites were not enhanced. More coherence in the O_3 enhancements at Hong Kong and the more northerly sites occurred toward the end of the episode (November 4–7), when modest enhancements in peak O_3 on at least 1 of the days were recorded at all four eastern sites.

A comparison between the average observed daily peak O_3 concentrations at each of the four eastern sites for the entire 3-month period (October 15, 1994, to January 15, 1995) and the late October/early November episode is presented in Figure 6. We find that episodic averages in peak O_3 concentrations were about 19, 12, 29, and 17 ppbv higher than their 3-month averages at Longfeng San, Qindao, Linan, and Hong Kong, respectively. By contrast, there was an approximate 1 ppbv difference between the episodic and 3-month average peak O_3 at Waliguan.

The fact that high O_3 concentrations were observed more or less simultaneously at sites separated by thousands of kilometers during the late October/early November episode suggests that it was being driven by a regional-scale process. The fact that the peak O_3 concentrations at the eastern monitoring sites during the episode were significantly larger than the nighttime concentrations observed at Waliguan for the entire 3-month period suggests that the O_3 concentration enhancements were caused by a boundary layer source such as photochemical production driven by the emissions of O_3-precursor pollutants. Support for these two inferences is provided in the next section where we show that the episode was associated with a synoptic-scale meteorological system conducive to the formation of O_3 pollution.

6. Meteorological Conditions During the Late October/Early November Episode

Figure 7 presents analyses of daily mean temperatures and (sea level) pressures on 4 representative days during the 13-day episode. At the beginning of the period (Figure 7a), high-pressure centers are located over western Mongolia and the East China Sea. Between these two centers a ridge of high pressure runs in a northeasterly/southwesterly direction over central China and the Yangtze Delta (where the Linan monitoring site was located). It is also noteworthy that the isobars during this early stage are oriented from south-southwest to north-northeast, suggesting a weak southwesterly flow and thus the advection of warm temperatures along the eastern seaboard.

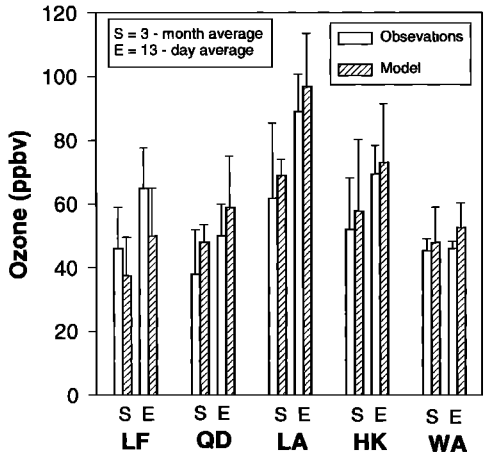

Figure 6. Comparison of observed and model-calculated average daily peak O_3 concentrations and their standard deviations for each of the five monitoring sites during the entire 3-month period (October 15, 1994, to January 15, 1995) and the 13-day late October/early November episode.

As the episode progresses, the maximum pressures to the northwest and southeast of the ridge remain fairly constant. However, the portion of the ridge that lies over eastern China tends to intensify and broaden. By October 31 (Figure 7b) the ridge of high pressure has spread over the entire eastern portion of China, and the 1024 hPa isobar line is seen to run along the eastern coastline from just north of Hong Kong to the northeastern corner of China. Over the next few days, when the highest peak O_3 concentrations were observed at Linan, Qindao, and Longfeng San, conditions over the region of interest remain fairly constant. On November 2 (Figure 7c) the ridge along the eastern seaboard is still quite broad but has receded from the northeastern corner of China in the face of a low-pressure trough pushing down from eastern Siberia. By November 5 (Figure 7d) the low-pressure trough has begun to dominate much of the northeastern portion of China, pinching off the high-pressure ridge along the coast, and signaling the decline of the episode.

Thus we find that the meteorological conditions over eastern China during the 13-day episode were highly conducive to the

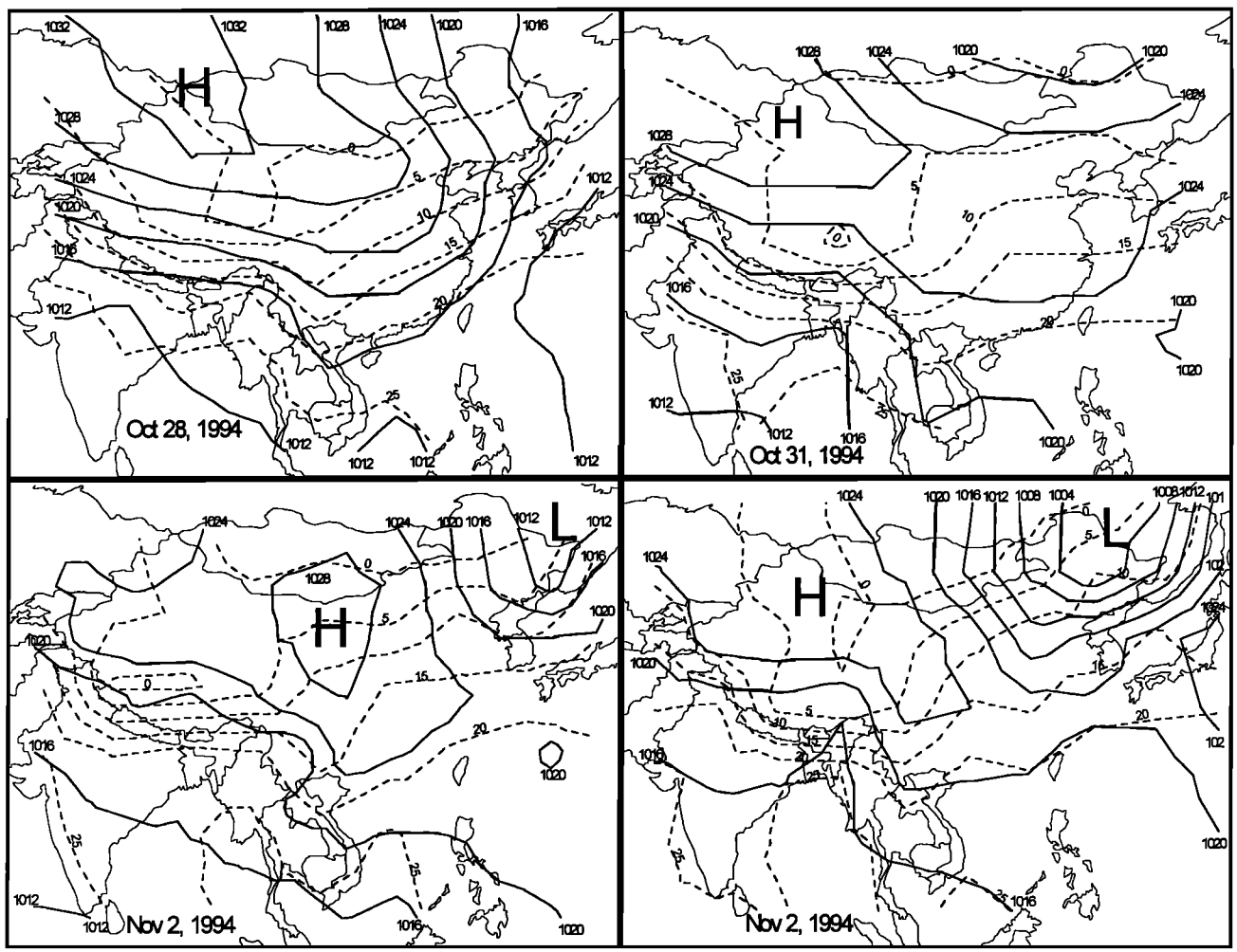

Figure 7. Analyses of pressure (hPa) and temperature (°C) over East Asia for 4 representative days during the late October/early November episode. The analyses are based on daily mean surface pressures (corrected to sea level) and temperatures measured at nearly 1000 surface meteorological stations in East Asia and acquired from the U.S. National Climatic Data Center's archive of "summary of the day" data sets. The data were rendered into synoptic surface charts using ArcView GIS™ and ARCView Spatial Analyst™ software. These software packages created isopleths of temperature and sea level pressure from the daily data by first gridding the data using inverse distance squared weighting, and then drawing contours using splines.

Table 1. Boundary Conditions Assumed for Simulations

Species[a]	Vertical Level					
	Level 1	Level 2	Level 3	Level 4	Level 5	Level 6
SO2	0.50	0.30	0.10	5.0×10^{-02}	2.0×10^{-02}	2.0×10^{-02}
SO4	0.20	0.10	7.0×10^{-02}	5.0×10^{-02}	4.0×10^{-02}	3.0×10^{-02}
NO2	0.30	0.20	0.15	7.0×10^{-02}	5.0×10^{-02}	4.0×10^{-02}
NO	2.0×10^{-02}	1.5×10^{-02}	1.0×10^{-02}	3.0×10^{-03}	1.0×10^{-03}	5.0×10^{-02}
O3	$3.0 \times 10^{+01}$	$3.5 \times 10^{+01}$	$4.0 \times 10^{+01}$	$4.5 \times 10^{+01}$	$6.0 \times 10^{+01}$	$9.0 \times 10^{+01}$
HNO3	0.10	5.0×10^{-02}	5.0×10^{-02}	5.0×10^{-02}	1.0×10^{-04}	1.0×10^{-04}
H2O2	1.0	1.0	0.50	0.30	0.20	0.20
ALD[b]	5.0×10^{-02}	5.0×10^{-02}	3.0×10^{-02}	3.0×10^{-02}	1.0×10^{-02}	5.0×10^{-03}
HCHO	0.15	0.15	0.10	0.10	5.0×10^{-02}	1.0×10^{-02}
PAA[c]	3.0×10^{-02}	3.0×10^{-02}	2.0×10^{-02}	1.0×10^{-02}	1.0×10^{-02}	5.0×10^{-03}
PAN[d]	0.10	0.10	6.0×10^{-02}	4.0×10^{-02}	3.0×10^{-02}	1.0×10^{-02}
H. alkanes[e]	0.40	0.40	3.0×10^{-02}	2.0×10^{-02}	1.0×10^{-02}	5.0×10^{-03}
Ethane	0.40	0.40	0.20	5.0×10^{-02}	1.0×10^{-02}	1.0×10^{-03}
CO	$1.0 \times 10^{+02}$	$1.0 \times 10^{+02}$	$9.0 \times 10^{+01}$	$8.0 \times 10^{+01}$	$7.0 \times 1^{+01}$	$6.0 \times 10^{+01}$
OL2[f]	5.0×10^{-02}	4.0×10^{-02}	2.0×10^{-02}	1.0×10^{-02}	5.0×10^{-03}	2.0×10^{-03}
OL3[g]	2.0×10^{-03}	1.0×10^{-03}	5.0×10^{-04}	1.0×10^{-4}	0.00	0.00
OL4[h]	1.0×10^{-04}	1.0×10^{-04}	1.0×10^{-04}	0.00	0.00	0.00
TOL[i]	2.0×10^{-02}	2.0×10^{-02}	7.0×10^{-03}	2.0×10^{-03}	5.0×10^{-03}	1.0×10^{-04}
XYL[j]	2.0×10^{-03}	2.0×10^{-03}	2.0×10^{-03}	0.00	0.00	0.00

Units are ppbv.
[a]See *Chang et al.* [1987] for definition of species.
[b]ALD, acetaldehydes and other aldehydes with two or more C atoms.
[c]PAA, peroxyatacetic acid.
[d]PAN, peroxyacetyl nitrate.
[e]H. alkanes, all alkanes containing three or more C atoms.
[f]OL2, ethylene.
[g]OL3, propylene.
[h]OL4, all other olefins.
[i]TOL, toluene and less reactiver aromatics.
[j]XYL, xylene and more reactive aromatics.

formation and accumulation of O_3 pollution over regional scales. They were also distinctly different from the strong frontal activity typically associated with tropopause folding events that bring O_3-rich air from the upper troposphere and lower stratosphere to the boundary layer [*Danielsen*, 1968]. The lack of strong synoptic forcing also argues against long-range, interregional transport of O_3 as the cause of the episode. The only viable explanation for the episode would appear to be photochemical; that is, the production of O_3 within the region from photochemical reactions driven by intraregional emissions of O_3 precursors, VOC, and NO_x, and the accumulation of this O_3 within the boundary layer. In order to ascertain if anthropogenic VOC and NO_x emissions from within China are, in fact, large enough to have generated the O_3 enhancements observed at the CORP sites and, if so, to characterize the sensitivity of the O_3 enhancements to changes in emissions, a series of regional air quality model simulations were carried out. These simulations are discussed below.

7. Model Description

An updated version of the Regional Acid Deposition Model (RADM) of *Chang et al.* [1987] was used to calculate three-dimensional concentration fields for O_3, its precursor species, and related free radical and other trace species over East Asia as a function of time for the 3-month period from October 15, 1994, to January 15, 1995. The model domain in the horizontal consisted of 83 × 71 grid cells in the east-west and south-north directions having dimensions of 60 km on a side placed on a Lambert conformal map (see Plate 1). The domain encompassed Japan and North and South Korea, as well as most of China. In the vertical direction the model was configured with six layers using a σ-coordinate system. The lowest three layers ($1 < \sigma < 0.98$; $0.98 < \sigma < 0.93$; $0.93 < \sigma < 0.86$) corresponded to heights of 0–0.16, 0.16–0.55, and 0.55–1.1 km and were typically in the planetary boundary layer during the day. The other three layers ($0.86 < \sigma < 0.67$; $0.67 < \sigma < 0.35$; $0.35 < \sigma$) corresponded to altitudes of 1.1–2.9, 2.9–6.9, and 6.9–15 km and were in the free troposphere. A time step of 150 s was employed for integration of both the chemical and transport tendency equations.

Our RADM application included an updated photochemical mechanism describing the production and loss of O_3 [*Demore et al.*, 1997], as well as a modified parameterization for subgrid-scale vertical transport. More specifically, vertical transport of chemical species occurring over spatial and timescales below model resolution was simulated using first-order closure eddy diffusion theory that parameterizes transport using a vertical eddy diffusion coefficient K_z. In the surface or first vertical layer, K_z was computed according to Monin-Obukov similarity theory [*Louis*, 1979; *Businger et al.*, 1971]. Above the surface layer but in the planetary boundary layer (i.e., layers 2 and 3), K_z was calculated using the method of *Wyngaard and Brost* [1984]. Above layer 3, K_z was determined using the method of *Blackadar* [1979]. Dry deposition of chemical species at the Earth's surface was simulated using the formulation of *Wesley and Hicks* [1977], with the relevant meteorological data from the RegCM simulation described below and land cover data from *Shieh et al.* [1979]. Boundary conditions for all chemical species affected by transport are listed in Table 1; in general, these were set to values normally associated with clean tropo-

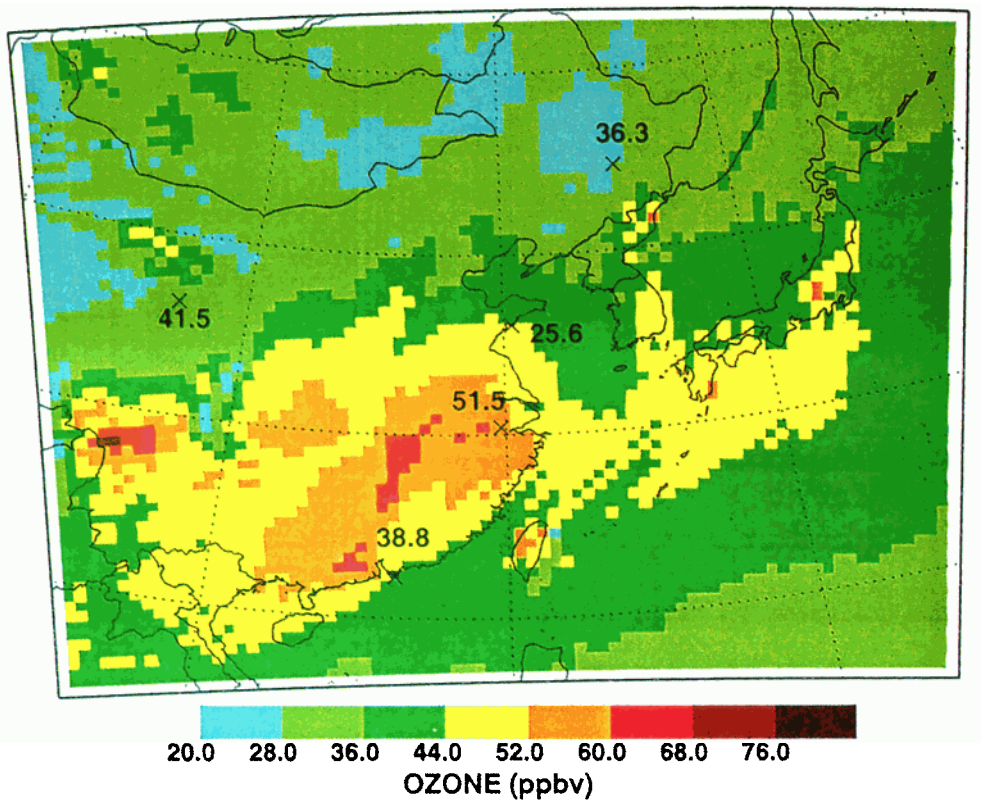

Plate 2. The spatial distribution in the 24-hour average O_3 concentration calculated by the model over the 3-month simulation period (color coding) with the observed O_3 averages at each of the five monitoring sites superimposed.

spheric air so that any concentration enhancements that might appear in the simulations could be attributed to processes occurring within the model domain.

To calculate O_3 photochemical production rates, the model must first calculate the concentrations of the O_3 precursor species, and this, in turn, requires specification of the precursor emissions as a function of location and time. In our 3-month simulation all emissions were assumed to be time-independent. Anthropogenic NO_x emissions, illustrated in Plate 1, were based on the annually averaged gridded inventories of *Bai* [1996] for China and *Kato and Akimoto* [1992] for Japan and North and South Korea. Total anthropogenic VOC and CO emissions were scaled relative to anthropogenic NO_x emissions. The CO:NO_x and VOC:NO_x emissions ratios adopted for the model domain lying outside of China were adopted from *Liu et al.* [1996]. For the model domain inside China the ratios of *Liu et al.* [1996] were revised for each province on the basis of fuel usage and source category statistics provided by the *State Statistical Bureau of China* (*SSBC*) [1990]. As the simulation was carried out for the fall and early winter months, biogenic VOC emissions were set to zero [*Guenther et al.*, 1995].

Before the total VOC emission inventories described above can be used in the model, they must first be speciated (i.e., the total VOC emissions must be divided into individual emission inventories for each relevant organic compound). In the case of RADM the relevant organic compounds are actually 10 generalized or surrogate compounds used in the model to represent the organic chemistry of the atmosphere [*Chang et al.*, 1987]. For the RADM application discussed here, we used four different sets of emissions splits. Outside of China the division of the emissions between the various surrogate compounds was prescribed using the ratios derived by *Liu et al.* [1996]. Within China we used an additional three sets of emissions splits for the northwestern, northeastern, and southern portions of the nation that fall within our model domain. In each case the splits were derived from speciated VOC measurements made at an nonurban monitoring site located in that portion of China during the 3-month simulation period [*Xu et al.*, 1996]. A listing of the emissions splits, the regions of China where they were adopted, and the site where the VOC speciation data were used to derive the splits for each region are presented in Table 2.

To simulate transport processes in RADM, time-dependent, three-dimensional meteorological fields must be specified; these include values for horizontal wind speed and direction, temperature, precipitation, water vapor concentration, and pressure. In our simulations these fields were taken from the appropriate 3-month portion of a simulation of East Asian meteorology from June 1994 to August 1995 using the National Center for Atmospheric Research (NCAR) Regional Climate Model (RegCM) [*Giorgi et al.*, 1993, 1999; *Qian and Giorgi*, 1999]. A comprehensive description and evaluation of the East Asian RegCM simulation used here is provided by *Giorgi et al.* [1999], and thus our discussion of the model and its results will be limited to the most salient points. The meteorological fields calculated by RegCM were saved at 6-hour intervals, interpolated to 150-s time intervals, and then input into RADM. As the RegCM simulation used the same horizontal grid as that used in our RADM simulation (with a

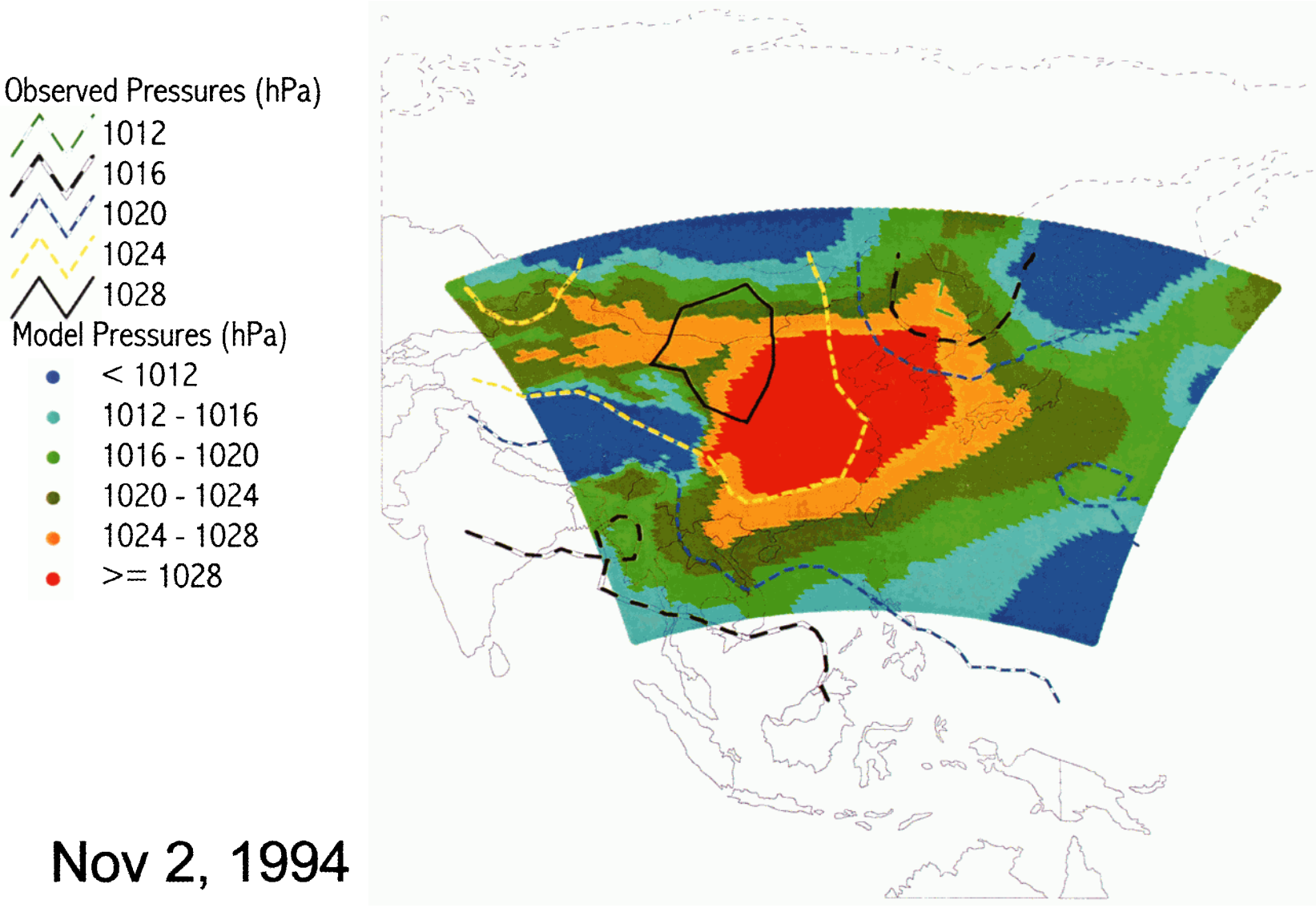

Plate 3. A comparison of an analysis of observed and RegCM-calculated daily mean sea level pressures on November 2, 1994. The procedures used to analyze observed pressures are described in the caption to Figure 7. The RegCM pressures were taken from the pressure calculated for the model's lowest vertical level and then corrected to sea level using standard procedures. (The reader should note that in the sea level correction of the RegCM pressures, "plateau factors" were not used, and thus a spurious low-pressure system appears over the Tibetan Plateau. As this area is not germane to our study, we have not attempted to correct for this artifact of the analysis.)

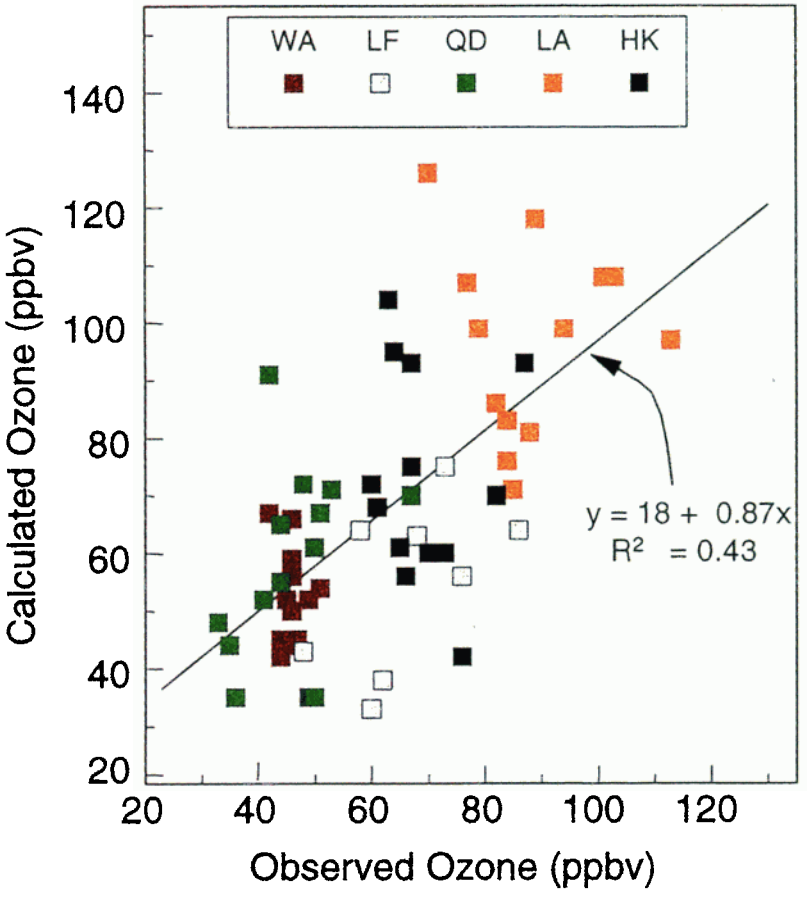

Plate 4. Scatterplot of observed and model-calculated daily maximum O_3 concentrations during the 13-day episode at the five monitoring sites (WA, Waliguan; LF, Longfeng San; QD, Qindao; LA, Linan; HK, Hong Kong). The regression is for the combined data from all sites.

slightly larger horizontal domain), no horizontal adjustment or interpolation of the RegCM fields was needed. On the other hand, the RegCM simulation used 14 levels in the vertical, while our RADM application only used 6 levels. Condensation of the 14-layer meteorological fields from RegCM into the 6-layer fields needed for RADM was accomplished using a sigma-weighted averaging.

8. Simulation of Ozone Concentrations

In this section we discuss the main features of the model-calculated O_3 fields and compare them with those inferred from the aforementioned data.

8.1. Average Spatial Distribution Over 3-Month Simulation Period

In Plate 2 we present the spatial distribution in the average concentration of O_3 calculated by the model over the 3-month simulation period, as well as the O_3 averages observed at each of the five monitoring sites in China. Model-calculated O_3 concentrations over the 3-month period are predicted to exceed the lower tropospheric concentrations assumed at the lateral boundaries of the model domain over much of China. Especially high O_3 enhancements are predicted over a large contiguous region that includes the middle portion of China's eastern coast, and then extends westward on a line centered along the Yangtze Delta and then southward along the Pearl River Delta to the southern coast on the South China Sea. Other, smaller pockets of enhanced O_3 concentrations are predicted in the Szechuan Basin and around Wuhan. The fact that the model-calculated O_3 enhancements tend to be most pronounced in the regions of China where precursor emissions are also relatively large (see Plate 1) suggests that they are being generated in the model by the photochemical smog process. This inference is confirmed by the fact that the enhancements in O_3 calculated by the model disappeared when the anthropogenic emissions over China were neglected.

A direct comparison between model-calculated and observed averages in daily maximum O_3 concentrations at the five monitoring sites is provided in Figures 6 and 8. These figures suggest that the distribution in O_3 over the 3-month simulation period predicted by the model is quite similar to the, albeit limited, O_3 observations. For example, note in Figure 6 that in both the observations and the model calculations, Lin An has the highest 3-month-averaged O_3 concentration of the five monitoring sites. Moreover, both observations and model calculations yield a 3-month average O_3 concentration at Lin An in the 60–70 ppbv range. As indicated in Figure 8, linear regression of the 3-month averages for all five monitoring sites yields a slope of 1 and an R^2 of 0.64. The value for the slope indicates that there is no significant overall bias in the model-calculated O_3 concentrations, and the R^2 value indicates that the model is capturing almost 65% of the spatial variability in average O_3 implied by the measurements, that is, an O_3 peak on the east coast in the Yangtze Delta region, somewhat higher

Table 2. Percentage of Total Anthropogenic VOC Emissions Within China Assigned to Each of the 10 Surrogate Species Used in the RADM Mechanism

Surrogate Species[a]	Subregion 1[b]	Subregion 2[c]	Subregion 3[d]
Ethane	16	10	10
H. Alkanes	16	10	10
OL2	13	24	26
OL3	13	24	25
OL4	12	24	25
TOL	14	3	1
XYL	14	3	1
ALD	1	1	1
HCHO	1	1	1
Isoprene	0	0	0
Total	100	100	100

[a]See *Chang et al.* [1987] and footnotes to Table 1 for definition of surrogate species.

[b]Subregion 1 included those parts of China north of 40°N latitude and west of 120°E. Emissions splits for this subregion were derived from speciated VOC data collected at Longfeng San.

[c]Subregion 2 included those parts of China lying within an area bordered by 35°N, 100°E on the southwest, 35°N, 105°E on the southeast, 40°N, 105°E on the northeast, and 40°N, 120°E on the northwest. Emissions splits for this subregion were derived from speciated VOC data collected at Waliguan.

[d]Subregion 3 included all parts of China not included in subregions 1 and 2. Emissions splits for this subregion were derived from speciated VOC data collected at Linan.

concentrations to the south of the Lin An site than to the north, and low to intermediate concentrations over much of the western portion of the nation. One aspect of the observations not captured by the model relates to the variation of O_3 along the eastern portion of China and north of the Lin An site. While the model predicts a monotonic decrease in O_3 as one moves northward from Lin An, the observations indicate lower concentrations in Qindao than in the northernmost site of Longfeng San. Thus the model overpredicts O_3 at Qindao and underpredicts O_3 at Longfeng San.

8.2. Temporal Variability and Simulation of Late October/Early November Episode

There is also a good deal of similarity between the observed and simulated temporal variability in O_3 illustrated in Figure 5. As in the case of the observations, the model-calculated O_3 concentrations at the four eastern monitoring sites are characterized by intermittent, generally multiday, air pollution episodes. By contrast, little variability in O_3 is seen at the western, Waliguan site (as one might expect because of its high altitude). In general, there are more model-calculated O_3 episodes than there are observed episodes, especially at Linan and Qindao. For Linan this apparent discrepancy may have been caused, at least in part, by the large gaps in the observed data from Linan. For Qindao, on the other hand, the larger number of model-calculated episodes reflects the systematic tendency noted above for the model to overpredict O_3 at that site.

A noteworthy feature of the results illustrated in Figure 5 is the fact that the model simulations, like the observations, show significant upward excursions in O_3 at each of the four eastern monitoring sites during the 13-day period from October 26 to November 7. The fact that the model correctly simulated the timing and spatial extent of the regional episode over China can be traced to the ability of the RegCM (whose meteorological fields were used to drive the RADM simulation) to reproduce the synoptic-scale stagnation that fostered the episode. This is illustrated in Plate 3, where we depict the RegCM-calculated and observed mean sea level pressures over the model domain on November 2, 1995. It is evident that the RegCM correctly simulates the key synoptic feature of the air pollution regional event, that is, the presence of a large high-pressure ridge over eastern China with little or no surface pressure gradients.

In addition to accurately simulating the timing of the late October/early November episode, the model also appears to

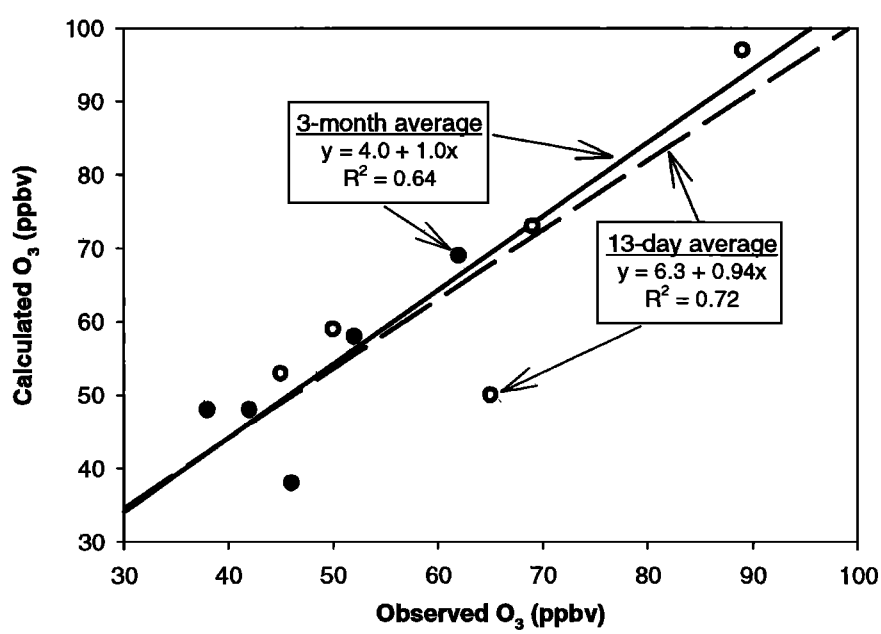

Figure 8. Scatterplots of observed and model-calculated averages in daily maximum O_3 concentrations at the five monitoring sites for the 3-month simulation period and for the 13-day late October/early November episode. The solid and dashed lines are the linear regressions for the 3-month and 13-day averages, respectively.

have reproduced much of the observed average behavior of O_3 at the monitoring sites during the episode. For example, note in Figure 8 that a linear regression between observed and model-calculated 13-day averages in daily peak O_3 at the five monitoring sites yields a slope of 0.9 and an R^2 of 0.72. From the more detailed, site-by-site comparison of the 13-day O_3 averages presented in Figure 6, we see that while differences in the absolute O_3 concentrations exist, the predicted O_3 enhancements during the 13-day episode are generally quite close to the observed enhancements, that is, observed and model-calculated enhancements of 12 and 11 ppbv at Qindao, 27 and 29 ppbv at Linan, 17 and 15 ppbv at Hong Kong, and 1 and 4 ppbv at Waliguan. In keeping with the model's tendency to underpredict O_3 at Longfeng San, the model-predicted enhancement at this site of 12 ppbv was less than the observed enhancement of 19 ppbv.

8.3. Simulation of Day-to-Day O_3 Variations

While model performance appears to be quite good when the metric for evaluation is multiday to monthly O_3 averages at the monitoring sites, the same cannot be said when the metric addresses day-to-day variations in O_3. For example, a linear regression between the model-calculated and observed daily maximum O_3 concentrations at each of the five monitoring sites for each of the 13 days of the episode yields an R^2 of 0.44 (see Plate 4). This would appear to suggest that the model is only capturing about 40% of the observed daily variation in O_3. In actuality, the model's simulation of the daily variability in O_3 is far weaker. More careful inspection of the data in Plate 4 indicates that most of the correlation between model calculations and observations arises from the model's relatively realistic simulation of the O_3 variations from site to site. However, for any of the sites the correlation between observed and model-calculated daily O_3 maxima is quite small. This result is fairly typical of regional air quality models (see, e.g., P. Kasibhatla and W. L. Chameides, Seasonal modeling of regional ozone pollution in the eastern United States, submitted to *Geophysical Research Letters*, 1999) and most likely reflects an inability of models of this scale to resolve subsynoptic-scale processes that drive day-to-day pollutant variability at a ground-level site during the stagnant conditions that typify air pollution episodes.

8.4. Simulation of Relationship Between O_3 and a Primary Pollutant: SO_2

Figure 9 compares the observed and model-predicted relationship between O_3 and SO_2, a primary pollutant that had been measured at three of the eastern monitoring sites. Data are shown for the entire 3-month period and for 5 days during the late October/early November episode when O_3 was generally at its highest at these sites. A summary of the linear regression statistics for each of the plots in Figure 9 is presented in Table 3.

First consider the scatterplots in Figures 9 based on the observed data (i.e., those along the left-hand side of the figure). Note that the observed relationships between O_3 and SO_2 change as we move from site to site, with a positive slope in two cases and a negative slope in the other; and with R^2 values ranging from about 0.2 to essentially 0. Also note that the data gathered at each site during the 5-day portion of the episode tend to cluster in one general area of each of the scatterplots. However, the area where these data cluster varies from one to site to another. Thus we find considerable variability in the observed relationships between O_3 and SO_2, and, as a result, comparison of these observed relationships with those derived from the model represents a nontrivial test of the model's proficiency and skill.

Inspection of the plots in Figure 9 derived from the model calculations indicates that the model is able to reproduce key elements of the observed relationships. For example, like the observed data, the model-simulated data from the 5-day portion of the late October/early November episode tend to cluster in specific regions of each of their respective scatterplots. Moreover, these regions tend to be qualitatively similar to the regions where the observed data appear in their scatterplots.

More quantitative comparisons summarized in Table 3 are also encouraging. Both the observations and model produce a positive slope of about 1.5 (ppbv O_3/ppbv SO_2) at Linan and a negative slope of about 0.6–0.8 (ppbv O_3/ppbv SO_2) at Qindao. On the other hand, the O_3-SO_2 slopes for Longfeng San are not consistent (a negative slope from the observations and a positive slope from the model). However, in this particular case, the R^2 values for both the observed and model-calculated data are quite small (i.e., 0.05 for the observations and 0.003 from the model). The very small R^2 values in these cases indicate that the slopes between O_3 and SO_2 at Longfeng San explain only a small fraction of the variability in these species (i.e., in both the observations and the model calculations, O_3 is essentially uncorrelated with SO_2 at Longfeng San). For this reason, the model calculations at Longfeng San are actually consistent with the observations at Longfeng San with respect to O_3 and SO_2, despite the differences in slopes.

8.5. Summary

While unable to simulate the observed day-to-day variability in O_3, the model appears to be able to reproduce the average spatial variability in O_3 over China on timescales of about 10 days to a few months. It also appears to be able to realistically simulate the overall response of O_3 at a location to the presence of synoptic-scale stagnation. Perhaps most importantly the model reproduces with reasonable fidelity the observed relationships between daily maxima in O_3 and the local daily concentrations of a primary pollutant, SO_2. These results suggest that the model is capturing many of the key chemical and meteorological processes that cause multiple-day high O_3 concentrations in nonurban locales in China, and thus could be used to estimate how these concentrations would respond, on average, to changes in precursor emissions. These estimates are presented in the next section.

9. NO_x Versus VOC Sensitivity

The photochemical mechanism responsible for O_3 production in the lower atmosphere is inherently nonlinear, and, as a result, the dependence of peak O_3 concentrations on its precurors, VOC and NO_x, can vary from one locale to another [*NRC*, 1991]. There are many factors that ultimately determine whether O_3 concentrations at a given locale are most sensitive to VOC emissions (i.e., VOC-limited conditions) or most sensitive to NO_x emissions (i.e., NO_x-limited conditions). These factors include (1) the VOC-to-NO_x ratio of the emissions; (2) the reactivity of the VOC emissions; (3) the meteorological conditions, which control the rate of transport of pollutants from source regions to rural areas; (4) the degree to which the VOC and NO_x emissions are spatially dispersed; and (5) the presence of biogenic VOC emissions. In the industrially devel-

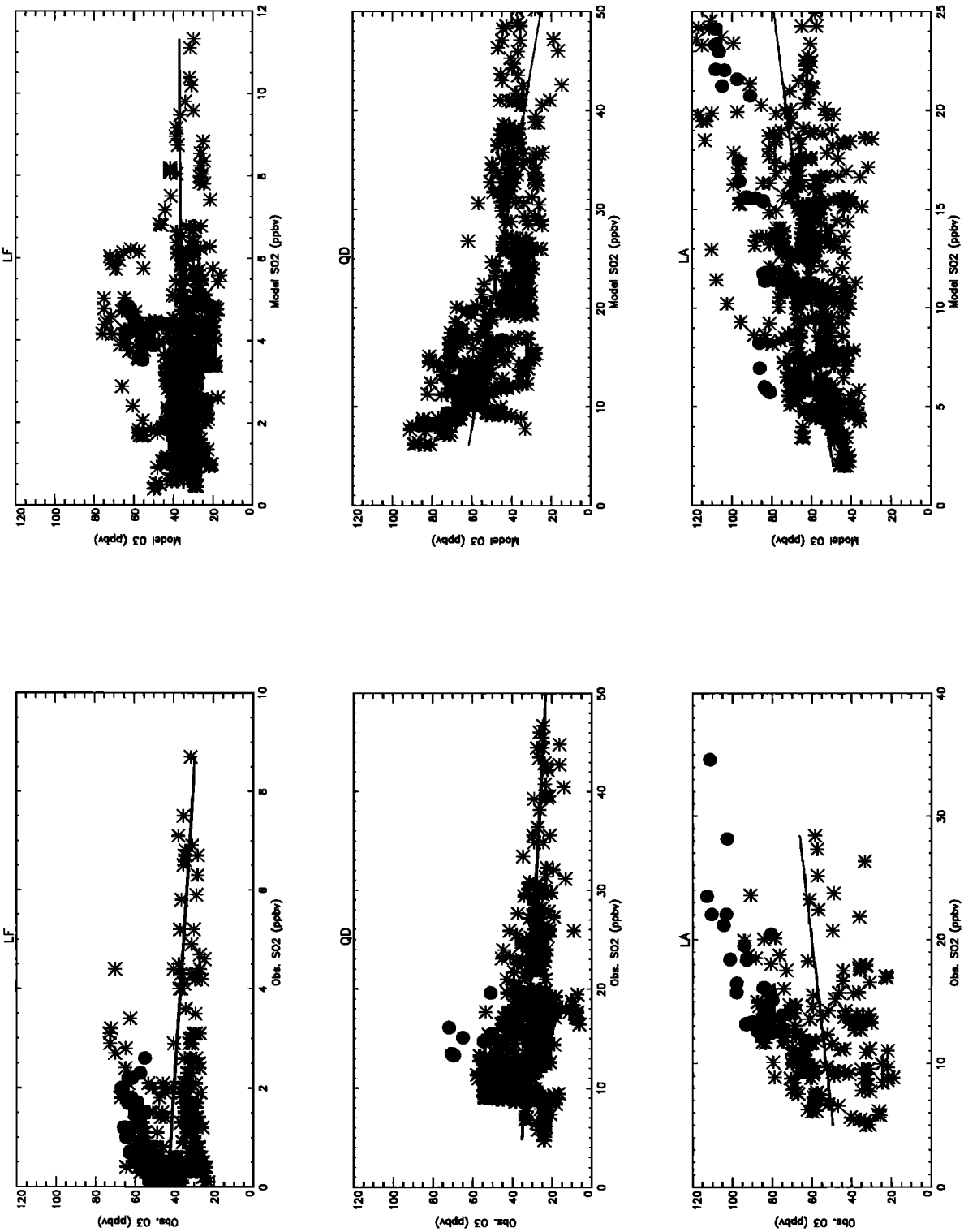

Figure 9. Scatterplots of daily maximum afternoon (1300–1800 hours local time) 1-hour averaged O_3 and SO_2 at Longfeng San (LF), Qindao (QD), and Lin An (LA). (left) Observations. (right) Model calculations. The dots are data points from October 30, 1994, to November 3, 1994, a 5-day period during the late October/early November episode when O_3 concentrations were generally at their height. The asterisks are for all other data from the 3-month simulation period.

Table 3. Linear Regression Statistics for Scatterplots of Observed and Model-Calculated Concentrations of O_3 Versus Sulfur Dioxide Concentrations

	Slope	Intercept	R^2
Linan			
Observations	1.61 ± 0.30	38.56 ± 20.62	0.14
Model	1.36 ± 0.09	47.09 ± 16.68	0.32
Longfeng San			
Observations	−1.58 ± 0.42	44.67 ± 11.61	0.05
Model	0.32 ± 0.26	35.02 ± 11.52	0.003
Qindao			
Observations	−0.62 ± 0.06	40.00 ± 12.26	0.23
Model	−0.82 ± 0.05	67.02 ± 12.90	0.36

Uncertainties are standard errors at the 95% confidence interval.

oped areas of the West, peak O_3 concentrations in, and in the immediate vicinity of, major urban and industrial centers are often found to be most sensitive to VOC emissions, while peak O_3 concentrations in more suburban and rural locations are usually most sensitive to NO_x emissions [*Chameides et al.*, 1992; *Trainer et al.*, 1993; *Sillman*, 1995; *Duncan and Chameides*, 1998]. However, this is by no means a hard and fast rule, and exceptions are not uncommon [e.g., *Chameides et al.*, 1988; *Jacob et al.*, 1996].

The similarity between the meteorological conditions documented here for a regional O_3 pollution episode in China and those typically encountered in the industrially developed areas of the West suggest that the VOC and NO_x sensitivity of peak O_3 concentrations in rural China during this episode may be similar to that found in the industrially developed areas of the West. However, an important difference exists; the fall and winter timing of the China episode.

In order to explore the response of model-predicted peak O_3 in China during the late October/early November episode to changes in NO_x and VOC, we carried out a series of simulations using varying emissions of NO_x and VOC. Each simulation used identical initial and boundary conditions and was run from October 30, 1994, to November 3, 1994, the 5-day period that generally corresponded to the height of the 13-day episode. Plate 5 compares the model-predicted average afternoon O_3 concentrations for the base case (i.e., using present-day estimated emissions) with those obtained from model simulations assuming either a 35% reduction in NO_x and or a 35% reduction in VOC emissions. (NO_x and VOC sensitivities implied by model simulations using prescribed increases of NO_x and VOC emissions were quite similar to those obtained from prescribed decreases and are not illustrated here.)

Plate 5 reveals a spatially varying response to the assumed changes in NO_x and VOC emissions. One aspect of this spatial variation relates to changes within a given latitude regime as one moves from relatively rural areas to major urban and industrial centers (e.g., from rural areas in the Yangtze Delta to the Shanghai metropolitan area). In this case, we find a tendency for the O_3 photochemistry to shift toward greater VOC limitation as one moves to the urban and industrial centers.

Another aspect of the spatial variation has a distinct latitudinal dependence, especially in eastern China. In the portion of eastern China lying north of the Yangtze Delta, VOC limitation generally applies; that is, a 35% reduction in VOC leads to significant reductions in afternoon O_3 (of ~10–20 ppbv), while a 35% reduction in NO_x tends to cause a relatively minor O_3 decrease, or even an increase in O_3. In rural areas south of the Yangtze Delta, on the other hand, NO_x limitation is generally found with a 35% decrease in NO_x leading to a larger O_3 decrease than that obtained from a 35% decrease in VOC (i.e., O_3 decreases of ~5–10 ppbv for the NO_x reduction and ~2–5 ppbv for the VOC reduction). Within the Yangtze Delta itself the chemistry tends to be transitional between VOC and NO_x limitation; that is, the decreases in O_3 from a VOC and a NO_x reduction are roughly equivalent.

Because the Yangtze Delta and the southern part of China are predicted to have the highest O_3 concentrations, it follows that those regions of China with the highest O_3 generally tend to be transitional or NO_x-limited. Exceptions to this tendency are those small pockets in southern China that surround major urban and industrial centers (e.g., Shanghai in the Yangtze Delta, Hong Kong in the Yellow River Delta, and Chengdu in the Szechuan Basin).

The reasons for this spatially varying response can be understood from an inspection of Plate 6, where we compare the sources of NO_x and odd-hydrogen ($OH + HO_2$) production within the boundary layer of the model domain for the period from October 30, 1994, to November 3, 1994. (The chemical production of odd-hydrogen was calculated in, and averaged over, the lowest three model layers to arrive at a boundary layer source.) In general, the relative magnitudes of the NO_x and odd-hydrogen sources determine whether NO_x or VOC limitation applies [*Kleinman*, 1991]. In areas where the NO_x source is greater than the odd-hydrogen source, there is an excess of NO_x. Under these conditions the primary free radical loss pathway involves reaction with NO_2

$$\text{(R1)} \qquad OH + NO_2 + M \rightarrow HNO_3 + M$$

and the production of O_3 becomes limited by the supply of VOC, whose oxidation leads to secondary production of odd-hydrogen. (Because the chemistry in this regime is characterized by low free radical concentrations, it is also referred to as the radical-limited regime.) In areas where the NO_x source is less than the odd-hydrogen source, there is an excess of free radicals. For these conditions, the primary free radical loss pathway occurs via

$$\text{(R2)} \qquad HO_2 + HO_2 + M \rightarrow H_2O_2 + M$$

and the production of O_3 becomes limited by the supply of NO_x. Thus those regions in Plate 6c where the NO_x source is greater than the odd-hydrogen source generally correspond to those regions indicated in Plate 5 to be VOC-limited. Conversely, the regions in Plate 6c where the NO_x source is less than the odd-hydrogen source generally correspond to the NO_x-limited regions in Plate 5.

The tendency for NO_x limitation to give way to VOC limitation as one moves from rural areas to major urban/industrial centers is a fairly typical outcome of regional air quality models [*Possiel and Cox*, 1993; *Roselle and Schere*, 1995] and can be understood in terms of the change in NO_x emissions rates. Note in Plate 6 that as we move from a rural area to a large source region, the odd-hydrogen source remains relatively constant while the NO_x source increases. It is the increase in the NO_x source that forces the swing toward VOC limitation.

The transition from NO_x limitation to VOC limitation indicated in Plate 5 as we move from rural areas in southern China to rural areas in the northern part of China is a far less common result. Inspection of Plate 6 reveals that, in this case, the

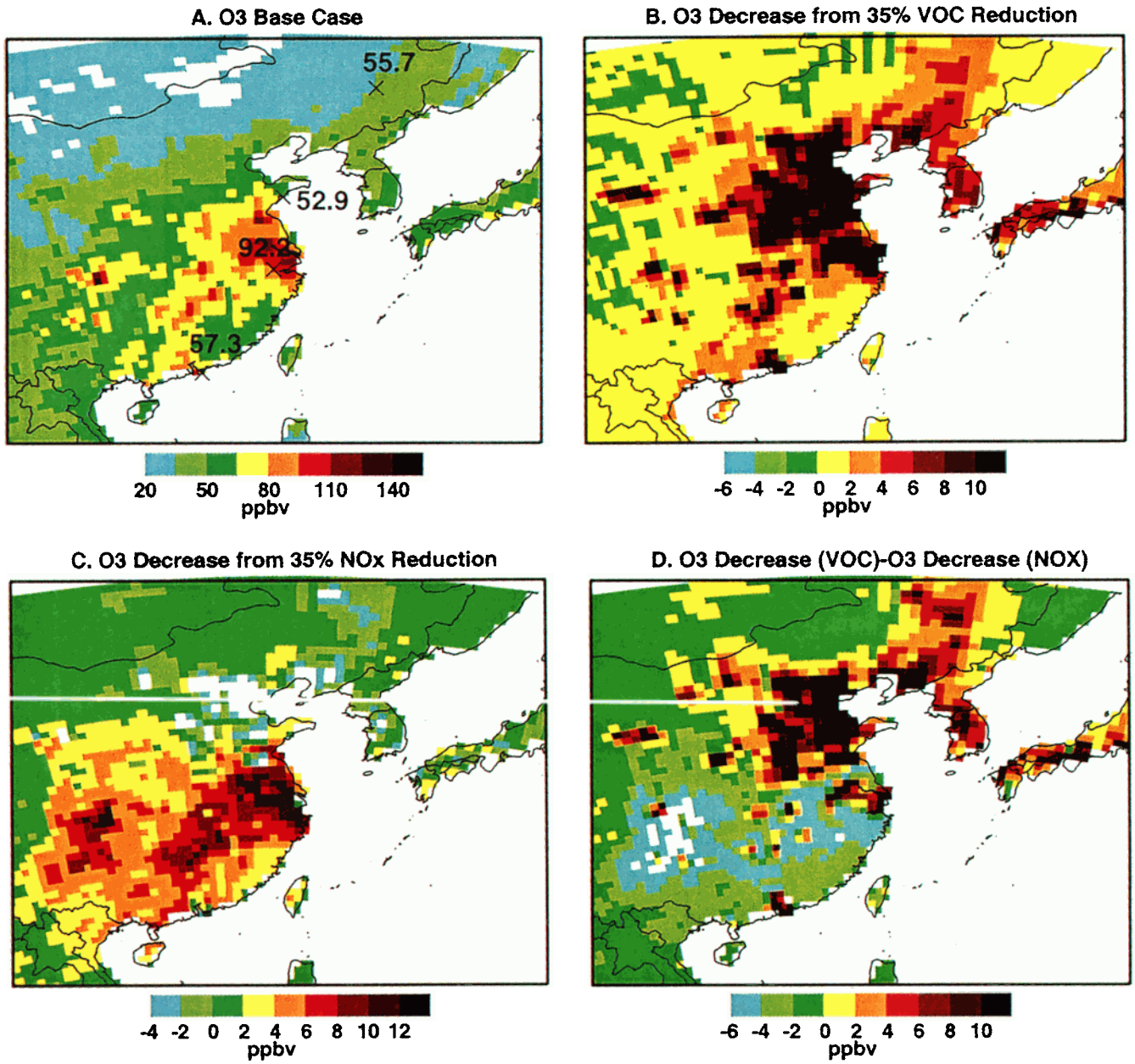

Plate 5. Comparison of model-predicted average afternoon O_3 concentrations over the period from October 30, 1994, to November 3, 1994, for three VOC and NO_x emissions scenarios. (a) Base case O_3 (i.e., using present-day estimated emissions). (b) Decrease in O_3 from the base case assuming 35% reduction in VOC. (c) Decrease in O_3 assuming 35% reduction in NO_x. (d) O_3 decrease from 35% reduction in VOC minus O_3 decrease from a 35% reduction in NO_x.

transition is caused by a decrease in the odd-hydrogen production rate as we move northward rather than an increase in the NO_x source. The decrease in the odd-hydrogen production rate with increasing latitude is, in turn, driven by photochemistry rather than anthropogenic emissions. A major contributor to the odd-hydrogen production rate is the primary production of OH radicals via the near-UV photolysis of O_3

(R3) $$O_3 + h\nu \rightarrow O(^1D) + O_2$$

followed by

(R4) $$O(^1D) + H_2O \rightarrow 2OH$$

As one moves to higher latitudes, the solar zenith angle increases, and this causes the solar flux capable of producing $O(^1D)$ from O_3 to decrease. Eventually the odd-hydrogen production rate becomes smaller than the NO_x production rate, and the O_3 photochemistry switches from being NO_x-limited to transitional and then to VOC-limited.

The fact that the latitudinal variation in the O_3 response to VOC and NO_x is driven by a variation in actinic flux with solar zenith angle has an interesting implication. The episode we have studied here took place in the late fall when the solar zenith angle over China is, on average, rather large, especially

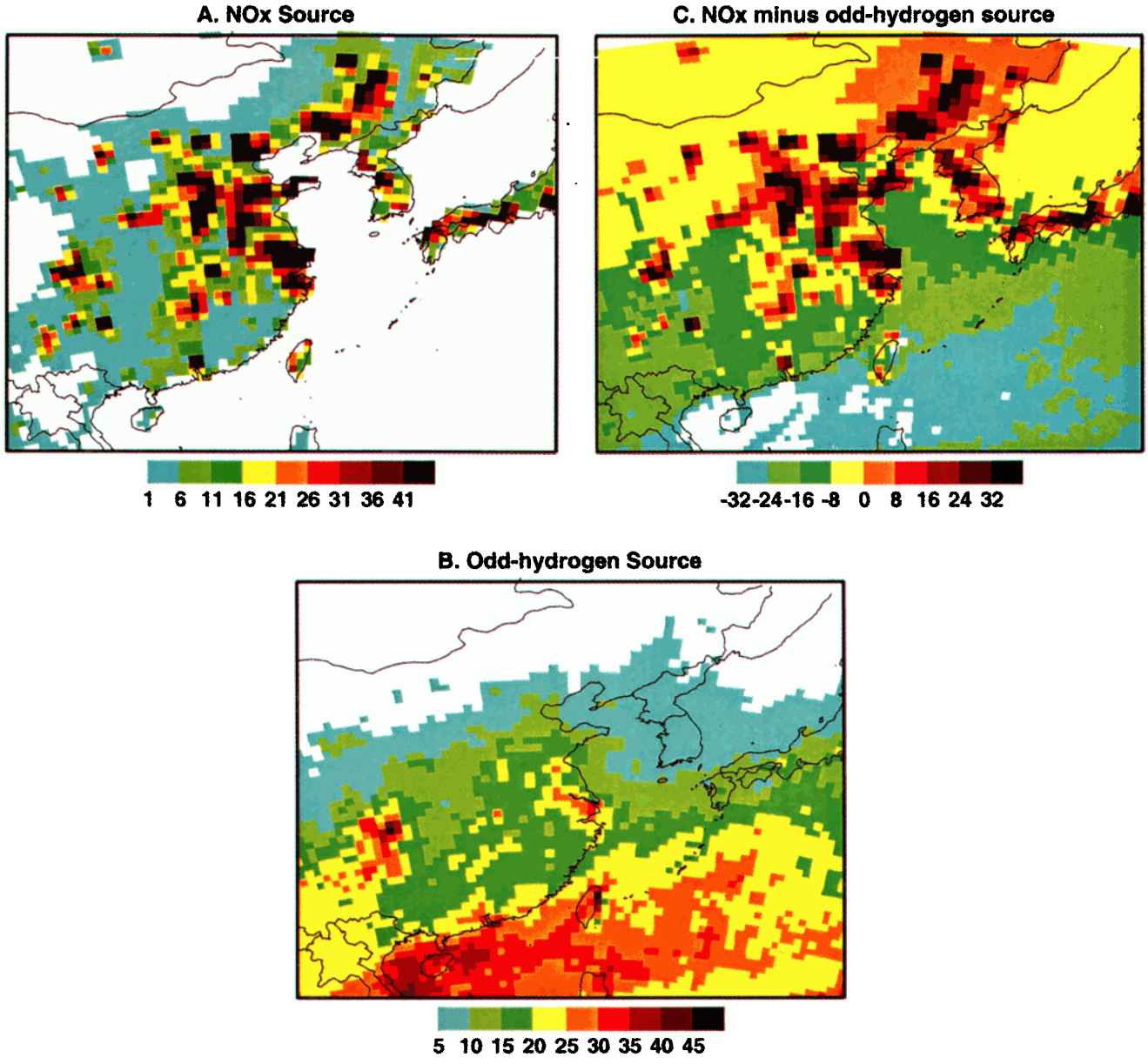

Plate 6. Comparison of boundary layer NO_x and odd-hydrogen sources for the period from October 30, 1994, to November 3, 1994. (Units are 1×10^5 molecules cm^{-3} s^{-1}.) The boundary layer NO_x source was calculated from the gridded NO_x emissions assuming a boundary layer height of 1.5 km. The boundary layer odd-hydrogen source was calculated in, and averaged over, the lowest three model layers to arrive at the boundary layer source.

at midlatitudes. It is conceivable that during the spring and summer seasons, when the Sun is higher in the sky and the odd-hydrogen production is higher throughout China, the transition to VOC limitation in northern China would no longer apply. In fact, *Jacobs et al.* [1995] found evidence for a similar seasonal transition in O_3 pollution episodes occurring in the Shenandoah region of Virginia.

10. Conclusion

On the basis of data collected at five nonurban sites in China over a 12-month period from August 1994 to August 1995, it appears that nonurban O_3 pollution episodes do occur in China and can, under the appropriate circumstances, extend over large regional scales. As is the case in the industrially developed regions of the West, these circumstances include the establishment of a high pressure ridge over the region. On the other hand, while major regional episodes in the United States and Canada as well as Europe most commonly occur during the summertime, the Asian Monsoonal Circulation appears to mitigate against summertime pollution episodes, and thus regional episodes in China were instead recorded during the fall and early winter.

An updated version of the Regional Acid Deposition Model (RADM) driven by meteorological fields derived from the Regional Climate Model (RegCM) has been found to reproduce many of the features of rural O_3 pollution observed over China during the late fall and early winter of 1994/1995. Well-simulated features included average O_3 concentrations, temporal and spatial variability, and relationships to primary pol-

lutants on timescales from several days to months. The model was also able to correctly predict the onset, persistence, and then dissipation of a regional nonurban O_3 pollution episode over China that occurred in late October and early November. However, day-to-day variability at a given site was poorly simulated, most likely because of the model's inability to resolve important subgrid-scale phenomena. This result is consistent with the analysis of a seasonal model simulation of regional O_3 in the eastern United States and suggests that regional models may be better suited to characterizing air quality phenomena over timescales of several days to months rather than on a daily basis.

Similar to regional-scale model simulations applied to the United States and Europe, our model calculations predicted a tendency for NO_x-limited chemistry in rural areas of China to transition to VOC-limited chemistry in the large urban and industrial centers where NO_x emission rates are largest. Our model also predicted a shift from NO_x-limited chemistry to VOC-limited chemistry in rural areas of China as one moves from low to high latitudes and actinic flux becomes increasingly limited. This is a result that is not characteristic of most other regional-scale model simulations, most likely because they are generally used to simulate summertime episodes when actinic flux is at a maximum.

The sensitivity of rural O_3 to both NO_x and VOC over the Yangtze Delta during the fall season, when rural O_3 concentrations appear to be at their highest, may forebode ill for China's rural air quality in the coming decades. The economy of the Yangtze Delta has been the most rapidly developing of all of China [*Heilig*, 1999]. If this economic expansion continues, the increased demand for energy will no doubt lead to significant increases in NO_x emissions. Our model simulations suggest that this will tend to make nonurban O_3 pollution in the region more severe. Perhaps even more critical, however, is the fact that as the region develops, it is expected that its economy will become less dependent upon coal and more dependent on oil as an energy source and will also rely more heavily on automobiles powered by internal combustion engines [*Elliott et al.*, 1997]. Both of these changes should lead to significant increases in VOC emissions, and our model simulations suggest that these increases will also exacerbate nonurban O_3 pollution.

Acknowledgments. This research was funded in part by the National Aeronautics and Space Administration under grant NAG5-3855 in support of the China-MAP Project and the National Science Foundation under grant ATM-9617378. The authors thank Filippo Giorgi for providing the RegCM model output, our Chinese colleagues who participated in the Chinese Ozone Research Program, supported by National Natural Science Foundation of China, and K. Baumann, R. Saylor, and P. Kasibhatla for their comments and suggestions.

References

Altschuller, A. P., S. L. Kopczynski, W. Lonneman, and D. Wilson, Photochemical reactivities of exhaust from 1966 model automobiles equipped to reduce hydrocarbon emission, *J. Air Pollut. Control Assoc.*, *17*, 734–737, 1967.

Bai, N. B., The emission inventory of CO_2, SO_2 and NO_x in China, in *The Atmospheric Ozone Variation and Its Effect on the Climate and Environment in China*, edited by Z. Xiuji, pp. 145–150, Meteorol. Press, Beijing, 1996.

Blackadar, A. K., High resolution models of the planetary layer, in *Advances in Environmental Science and Engineering*, edited by J. R. Pfafflin and E. N. Ziegker, pp. 50–85, Gordon and Breach, Newark, N. J., 1979.

Businger, J. A., J. C. Wyngaard, Y. Izumi, and E. F. Bradley, Flux-profile relationship in the atmospheric surface layer, *J. Atmos. Sci.*, *28*, 181–189, 1971.

Cardelino, C. A., and W. L. Chameides, Natural hydrocarbons, urbanization, and urban ozone, *J. Geophys. Res.*, *95*, 13,971–13,979, 1990.

Chameides, W. L., R. W. Lindsay, J. Richardson, and C. S. Kiang, The role of biogenic hydrocarbons in urban photochemical smog: Atlanta as a case study, *Science*, *241*, 1473, 1988.

Chameides, W. L., et al., Ozone precursor relationships in the ambient atmosphere, *J. Geophys. Res.*, *97*, 6037–6055, 1992.

Chameides, W. L., P. S. Kasibhatla, J. Yienger, and H. Levy, Growth of continental scale Metro-Agro-Plexes, regional ozone pollution and world food production, *Science*, *264*, 74–77, 1994.

Chameides, W. L., et al., Is ozone pollution affecting crop yields in China?, *Geophys. Res. Lett.*, *26*, 867–870, 1999.

Chang, J. S., R. A. Brost, I. S. Isaksen, S. Madronich, P. Middleton, W. R. Stockwell, and C. J. Walcek, A three-dimensional Eulerian acid deposition model: Physical concepts and formulation, *J. Geophys. Res.*, *92*, 14,681–14,700, 1987.

Danielsen, E. F., Stratospheric-tropospheric exchange based upon radioactivity, ozone and potential vorticity, *J. Atmos. Sci.*, *25*, 502–518, 1968.

Davies, T. D., P. M. Kelly, P. S. Low, and C. E. Pierce, Surface ozone concentrations in Europe: Links with the regional-scale atmospheric circulation, *J. Geophys. Res.*, *97*, 9819–9832, 1992.

Davis, J. M., B. K. Eder, D. Nychka, and Q. Yang, Modeling the effects of meteorology on ozone in Houston using cluster analysis and generalized additive models, *Atmos. Environ.*, *32*, 2505–2520, 1998.

Demore, W. B., C. J. Howard, A. R. Ravishankara, M. J. Molina, D. M. Golden, C. E. Kolb, R. F. Hampson, and M. J. Kurylo, Chemical kinetics and photochemical data for use in stratospheric modeling, *JPL Publ.*, *97-4*, 1997.

Ding, Y., Summer monsoon rainfalls in China, *Meteorol. Soc. Jpn.*, *373*, 243, 1992.

Dodge, M. C., A comparison of three photochemical oxidant mechanisms, *J. Geophys. Res.*, *94*, 5121–5136, 1989.

Duncan, B. N., and W. L. Chameides, Effects of urban emission control strategies on the export of ozone and ozone precursors from the urban atmosphere to the troposphere, *J. Geophys. Res.*, *103*, 28,159–28,179, 1998.

Elliott, S., D. R. Blake, R. A. Duce, C. A. Lai, I. McCreary, L. A. McNair, F. S. Rowland, and A. G. Russell, Motorization of China implies changes in Pacific air chemistry and primary production, *Geophys. Res. Lett.*, *24*, 2671–2674, 1997.

Fishman, J. F., M. Vukovich, D. R. Cahoon, and M. C. Shipham, The characterization of an air pollution episode using satellite total ozone measurements, *J. Clim. Appl. Meteorol.*, *26*, 1638–1654, 1987.

Galloway, J. D., H. Levy, and P. S. Kasibhatla, Year 2000: Consequences of population growth and development on deposition of oxidized nitrogen, *Ambio*, *23*, 120–123, 1994.

Giorgi, F., M. R. Marinucci, and G. T. Bates, Development of a second-generation regional climate model (RegCM2), part I, Boundary-layer and radiative transfer processes, *Mon. Weather Rev.*, *121*, 2794, 1993.

Giorgi, F., Y. Huang, K. Nishizawa, and C. Fu, A seasonal cycle simulation over East Asia and its sensitivity to radiative transfer and surface processes, *J. Geophys. Res.*, *104*, 6403–6423, 1999.

Grotjahn, R., *Global Atmospheric Circulations—Observations and Theories*, 430 pp., Oxford Univ. Press, New York, 1993.

Guenther, A., et al., A global model of natural volatile organic compound emissions, *J. Geophys. Res.*, *100*, 8873–8892, 1995.

Haagen-Smit, A. J., and M. M. Fox, Ozone formation in photochemical oxidation of organic substances, *Ind. Eng. Chem.*, *48*, 1484–1487, 1956.

Heilig, G. K., *Can China Feed Itself?*, ChinaFood CD-ROM Version 1.1, Int. Inst. for Appl. Syst. Anal. Land Use Change (IIASA LUC) Proj., Laxenburg, Austria, 1999.

Jacob, D. J., L. W. Horowitz, J. W. Munger, B. G. Heikes, R. R. Dickerson, R. S. Artz, and W. C. Keene, Seasonal transition from NO_x- to hydrocarbon-limited conditions for ozone production over the eastern United States in September, *J. Geophys. Res.*, *100*, 9315–9324, 1995.

Jacob, D. J., et al., Origin of ozone and NO_x in the tropical troposphere: A photochemical analysis of aircraft observations over the South Atlantic basin, *J. Geophys. Res.*, *101*, 24,235–24,250, 1996.

Kato, N., and H. Akimoto, Anthropogenic emissions of SO_2 and NO_x

in Asia: Emission inventories, *Atmos. Environ., Part A, 26*, 2997–3017, 1992.

King, W. J., and F. M. Vukovich, Some dynamic aspects of extended air pollution episodes, *Atmos. Environ., 16*, 1171–1181, 1982.

Kleinman, L. I., Seasonal dependence of boundary layer peroxide concentrations: The low and high NO_x regimes, *J. Geophys. Res., 96*, 20,721–20,733, 1991.

Korth, M. W., Dynamic irradiation chamber tests of automotive exhausts, *Public Health Serv. Publ., 999-AP-5*, 1963.

Lefohn, A. S., *Surface Level Ozone Exposures and Their Effects on Vegetation*, 350 pp., A. F. Lewis, New York, 1992.

Liu, S. C., et al., Model study of tropospheric trace species distributions during PEM-West A, *J. Geophys. Res., 101*, 2073–2085, 1996.

Logan, J. A., Rural ozone in the United States, *J. Geophys. Res., 94*, 8511–8532, 1989.

Louis, J. F., A parametric model of vertical eddy fluxes in the atmosphere, *Boundary Layer Meteorol., 17*, 187–207, 1979.

Millán, M. R., R. Salvador, E. Matilla, and B. Artíñano, Meteorology and photochemical air pollution in southern Europe: Experimental result form EC research projects, *Atmos. Environ., 30*, 1909–1924, 1996.

National Research Council, *Rethinking the Ozone Problem in Urban and Regional Air Pollution*, 50 pp., Natl. Acad. Press, Washington, D. C., 1991.

Peng, Y., C. Luo, X. Xu, R. Xiang, G. Ding, J. Tang, M. Wang, and X. Yu, The study of distribution characters of O_3, NO_x and SO_2 at rural areas in China, *Q. J. Appl. Meteorol., 8*, 53–60, 1997.

Possiel, N. C., and W. M. Cox, Relative effectiveness of NO_x and VOC strategies in reducing northeast U.S. ozone concentrations, *Water Air Soil Pollut., 67*, 161–179, 1993.

Roselle, S. J., and K. L. Schere, Modeled response of photochemical oxidants to systematic reductions in anthropogenic volatile organic compound and NO_x emissions, *J. Geophys. Res., 100*, 22,929–22,941, 1995.

Samson, P. J., and B. Shi, A meteorological investigation of high ozone in American cities, Office of Technology Assessment report, U.S. Govt. Print. Off., Washington, D. C., 1989.

Scheel, H. E., et al., Spatial and temporal variability of tropospheric ozone over Europe, in *Tropospheric Ozone Research, Transport and Chemical Transformation of Pollutants in the Troposphere*, edited by O. Hov, pp. 35–64, Spring-Verlag, New York, 1997.

Secretaria de Medio Ambiente, Recursos Naturales y Pesca (SEMARNAP), Primer informe sobre la calidad del aire en ciudades Mexicanas, 96 pp., Inst. Nac. de Ecol., Cent. Press Int., Mexico D.F., 1997.

Shieh, C. M., M. L. Wesley, and B. B. Hicks, Estimated dry deposition velocities over the northeastern United States, *Atmos. Environ., 13*, 1361–1368, 1979.

Sillman, S., The use of NO_y, H_2O_2, and HNO_3, as indicators for ozone-NO_x-hydrocarbon sensitivity in urban locations, *J. Geophys. Res., 100*, 14,175–14,188, 1995.

Sillman, S., J. A. Logan, and S. C. Wofsy, The sensitivity of ozone to nitrogen oxides and hydrocarbons in regional ozone episodes, *J. Geophys. Res., 95*, 1837–1851, 1990.

Smil, V., *China's Environmental Crisis: An Inquiry Into the Limits of National Development, An East Gate Book*, 257 pp., M. E. Sharpe, Armonk, N. Y., 1993.

State Statistical Bureau of China (SSBC), *The Yearbook of Energy Statistics of China 1989* (in Chinese), China Stat. Publ. House, Beijing, 1990.

Tang, X., J. Li, Z. Dong, W. Wang, X. Zhang, Y. Zhang, B. Tien, and L. Yang, Photochemical pollution in Lanzhow, China—A case study, paper presented at 79th Annual Meeting of the Air Pollution Control Association, Minneapolis, Minn., June 22–27, 1986.

Trainer, M., et al., Correlation of ozone with NO_y in photochemically aged air, *J. Geophys. Res., 98*, 2917–2925, 1993.

United Kingdom (U.K.) Report, Ozone in the United Kingdom, fourth report of the Photochemical Oxidants Review Group, 234 pp., London, 1997.

United Nations (U. N.), Agrostat-PC: Production, Comput. Inf. Ser. Food and Agric. Org., Rome, 1991.

U.S. Environmental Protection Agency (EPA), National air quality and emissions trends report, 1996, *EPA 454/R-97-013*, 152 pp., Off. of Air Qual. Plann. and Stand., Research Triangle Park, N. C., 1998.

Vukovich, F. M., A note on air quality in high pressure systems, *Atmos. Environ., 13*, 255–265, 1979.

Vukovich, F. M., Boundary layer ozone variations in the eastern United States and their association with meteorological variations: Long-term variations, *J. Geophys. Res., 99*, 16,839–16,850, 1994.

Vukovich, F. M., Regional-scale boundary layer ozone variations in the eastern United States and their association with meteorological variations, *Atmos. Environ., 29*, 2259–2273, 1995.

Vukovich, F. M., W. D. Bach, B. W. Crissman, and W. J. King, On the relationship between high ozone in the rural boundary layer and high pressure systems, *Atmos. Environ., 11*, 967–983, 1977.

Wang, T., K. S. Lam, L. Y. Chan, A. S. Y. Lee, and M. A. Carroll, Trace gas measurements in coastal Hong Kong during the PEM-West B, *J. Geophys. Res., 102*, 28,575–28,588, 1997.

Wang, T., K. S. Lam, A. S. Y. Lee, S. W. Pang, and W. S. Tsui, Meteorological and chemical characteristics of the photochemical ozone episodes observed at Cape D'Aguilar in Hong Kong, *J. Appl. Meteorol., 37*, 1167–1178, 1998.

Wesley, M. L., and B. B. Hicks, Some factors that affect the deposition rates of sulfur dioxide and similar gases on vegetation, *J. Air Pollut. Control, 27*, 1110–1116, 1977.

Wolff, G. T., and P. J. Lioy, Development of an ozone river associated with synoptic scale in the eastern United States, *Environ. Sci. Technol., 14*, 1257–1260, 1980.

Wyngaard, J. C., and R. A. Brost, Top-down and bottom-up diffusion of a Scalar in the convective boundary layer, *J. Atmos. Chem., 41*, 102–112, 1984.

Xu, X., Y. Xian, G. Ding, and X. Li, *Atmospheric Ozone Variations and Its Effect on the Climate and Environment in China*, edited by X. Zhou, pp. 67–81, Meteorol. Press, Beijing, 1996.

Qian, Y., and F. Giorgi, Interactive coupling of regional climate and sulfate aerosol models over eastern Asia, *J. Geophys. Res., 104*, 6477–6499, 1999.

W. L. Chameides, C. Luo, and J. C. St. John, School of Earth and Atmospheric Sciences, Georgia Institute of Technology, Atlanta, GA 30332. (wlc@blond.eas.gatech.edu)

K. S. Lam and T. Wang, Department of Civil and Structural Engineering, Hong Kong Polytechnic University, Hong Kong, China.

Z. Xiuji, Chinese Academy of Meteorological Sciences, Beijing 100081, China.

(Received April 5, 1999; revised September 7, 1999;
accepted September 11, 1999.)